and the culture dishes was transferred back to the CO_2 incubator. For passage, the old medium was removed and DPBS was pipetted onto the dishes under gentle shaking. After washing in DPBS, AutoCulture® supplied trypsin, oscillated the culture dishes, and returned them to the CO_2 incubator for a 5-min incubation. Following this, the robot arm moved the culture dishes onto the rotation table, added a prespecified volume of the basic culture media, and transferred the cell suspension from each dish to a separate 50-ml centrifuge tube. The cell suspension was centrifuged at 200 × *g* for 5 min at room temperature, and the supernatant was discarded. Fresh basic culture medium was supplied to the cell pellet, which was then resuspended. The washed cell suspension was subcultured at approximately 1:10 onto new culture dishes and returned to the CO_2 incubator.

Reverse transcription-polymerase chain reaction (RT-PCR)

Total RNA was extracted from cell populations containing CSCs, from human iPSCs, and raw human heart tissue samples using the RNeasy Plus Mini Kit (QIAGEN) as positive/negative control. Total RNA from human iPSCs and the human heart (Clontech Laboratories) was used as the positive control for each primer. Total RNA (500 ng per reaction) was converted to cDNA using the Transcriptor High Fidelity cDNA Synthesis Kit (Roche Applied Science) according to the manufacturer's protocol. Primers for the cardiac-specific transcription factors *NKX2.5* and *GATA4*; the stem cell markers *NANOG*, *OCT3/4*, *SOX2*, and *REX1*; and the housekeeping gene *GAPDH* were obtained from PrimerBank (Additional file 5).

Flow cytometric analysis

The cells (1×10^6 per reaction) were stained in autoMACS Running Buffer (Miltenyi Biotec.) with fluorescence-conjugated primary antibodies for 30 min at 4°C. The cells were then analyzed on the Attune Acoustic Focusing Cytometer (Applied Biosystem), and the data were analyzed using FlowJo 8.8.7 software (TOMY Digital Biology). Antibodies used for phenotyping included anti-human CD29-PE, CD90-PE, CD105-FITC, STRO-1-FITC, CD45-PE, and MHC class II-PE. Isotype controls were FITC-conjugated mouse IgG_1, PE-conjugated mouse IgG_1, and FITC-conjugated mouse IgM.

Lectin microarray analysis

Proteins were extracted from each cell population in hydrophobic and hydrophilic fractions using the CelLytic MEM Protein Extraction Kit (Sigma-Aldrich), as described previously [29]. Lectin microarray analysis was performed as described previously, with only minor modifications [30]. The glycoprotein (200 ng) was labeled with Cy3 monoreactive dye (GE Healthcare) in DPBS containing 0.5% Triton X-100 (PBSTx) at room temperature for 1 h. The Cy3-labeled glycoprotein solution (60 μl) was applied to the LecChip (GP Bioscience), which has triplicate spots specific for 45 lectins on each glass slide. An evanescent-field fluorescence scanner (GlycoStationTM Reader) was used to analyze the LecChip. All data were analyzed with GlycoStationTM Tools Signal Capture 1.0 and GlycoStationTM Tools Pro 1.0 software (GP Bioscience). To expand the dynamic range, the data were subjected to a gain-merging procedure, and the merged data were then normalized with max-normalization, as described previously [29].

aCGH analysis

Genomic DNA from the heart tissue and cultured cells was isolated using the DNeasy Blood & Tissue Kit (QIAGEN). Labeled test and reference DNAs were combined, denatured, preannealed with Cot-1 DNA (Invitrogen) and blocking agent, and then hybridized to the arrays (SurePrint G3 Human CGH Microarray 2x400K, Agilent Technologies). After hybridization and washing, the arrays were scanned at 3-μm resolution using an Agilent G2505C scanner. Images were analyzed with Feature Extraction software 10.7.3.1 (Agilent Technologies) using the CGH 107 Sep09 protocol for background subtraction and normalization.

Gene expression analysis

Gene expression analysis was performed using the Agilent Whole Human Genome Microarray chip G4112F (Agilent Technologies), which contains >41,000 probes. Raw data were normalized and analyzed by GeneSpring GX11 software (Silicon Genetics). Pairwise scatter plot analysis of the global gene expression profiles of both manually cultured cells and autocultured cells was performed on day 7 after thawing. The number of differentially expressed genes is indicated over each scatter plot. The NIA Array [18] web tool was used for pairwise scatter plot analysis. Gene expression microarray data have been submitted under accession number GSE 44032. Analysis of microarray experiments was conducted using the Aberration Detection Method-2 statistical algorithm (Agilent Technologies) on the basis of the combined log2 ratios at a threshold of 6.0. The data were centralized, and calls with average log2 ratios <0.3219 were filtered to exclude false positives.

Additional files

Additional file 1: Document 1. Specialization of the automated cell processing machine (Auto Culture®).

Additional file 2: Document 2. *Quantitative cellular aspects for* ALCADIA clinical trial.

Additional file 3: Table S1. Results of microarray analysis of CSCs in manual culture and AutoCulture®. To investigate the differences in global gene expression profile between CSCs in manual culture and CSCs in AutoCulture®, we performed a pairwise comparison of gene expression

microarray data using NIA array analysis. The results revealed similar gene expression patterns between them.

Additional file 4: Movie 1. AutoCulture®.Movie of the culture robot in AutoCulture®.

Additional file 5: Table S2. RT-PCR primer sequences. RT-PCR primer sequences were obtained from PrimerBank (http://pga.mgh.harvard.edu/primerbank/).

Abbreviation

CSC: Cardiac stem cells; FACS: Fluorescence-activated cell sorting; MSCs: Mesenchymal stem cells; aCGH: Array comparative genomic hybridization; RAA: Right atrial appendage; cGMP: Current good manufacturing practice; SOPs: Standard operating procedures; cGTP: Current good tissue practice; bFGF: Basic fibroblast growth factor.

Competing interests

DK, MYI, KM, TK, YI, MT, AU and SG declare that they have no competing interests. KW and TS are employees of Kawasaki Heavy Industries, Ltd.

Authors' contributions

DK, MT, AU, and SG designed the research; DK, KW, YI, KM, MYI, and performed the experiments; DK, MT, and SG analyzed the data; and DK, TK, YI, and SG wrote the manuscript. All authors read and approved the final manuscript.

Acknowledgments

We would like to express our sincere thanks to Nakata M. (Kyoto Prefectural University of Medicine) and Akutsu H (National Center for Child Health and Development). This research was supported by grants from Ministry of Education, Culture Sports, Science and Technology (MEXT) of Japan.

Author details

[1]Department of Regenerative Medicine, Kyoto Prefectural University of Medicine, 465 Kajii-cho, Kawaramachi-Hirokoji, Kamigyo-ku, Kyoto 602-8566, Japan. [2]System Technology Development Center, Kawasaki Heavy Industries, Ltd., 3-1-1 Higashi Kawasaki-cho, Chuo-ku, Kobe 650-8670, Japan. [3]Department of Reproductive Biology and Pathology, National Center for Child Health and Development, 2-10-1 Okura, Setagaya-ku, Tokyo 157-8535, Japan. [4]Department of Cardiovascular Medicine, Kyoto Prefectural University of Medicine, 465 Kajii-cho, Kawaramachi-Hirokoji, Kamigyo-ku, Kyoto 602-8566, Japan. [5]Department of Vascular Medicine, Tokyo Metropolitan Institute of Gerontology, 35-2 Sakae-cho, Itabashi-ku, Tokyo 173-0015, Japan.

Received: 7 May 2013 Accepted: 12 November 2013
Published: 15 November 2013

References

1. Takehara N, Tsutsumi Y, Tateishi K, Ogata T, Tanaka H, Ueyama T, Takahashi T, Takamatsu T, Fukushima M, Komeda M, *et al*: **Controlled delivery of basic fibroblast growth factor promotes human cardiosphere-derived cell engraftment to enhance cardiac repair for chronic myocardial infarction.** *J Am Coll Cardiol* 2008, **52**(23):1858–1865.
2. Smith RR, Barile L, Cho HC, Leppo MK, Hare JM, Messina E, Giacomello A, Abraham MR, Marban E: **Regenerative potential of cardiosphere-derived cells expanded from percutaneous endomyocardial biopsy specimens.** *Circulation* 2007, **115**(7):896–908.
3. Rota M, Padin-Iruegas ME, Misao Y, De Angelis A, Maestroni S, Ferreira-Martins J, Fiumana E, Rastaldo R, Arcarese ML, Mitchell TS, *et al*: **Local activation or implantation of cardiac progenitor cells rescues scarred infarcted myocardium improving cardiac function.** *Circ Res* 2008, **103**(1):107–116.
4. Vogel G: **Stem cells for sale.** *Science* 2010, **330**(6008):1173.
5. Tran CA, Burton L, Russom D, Wagner JR, Jensen MC, Forman SJ, DiGiusto DL: **Manufacturing of large numbers of patient-specific T cells for adoptive immunotherapy: an approach to improving product safety, composition, and production capacity.** *J Immunother* 2007, **30**(6):644–654.
6. Soncin S, Lo Cicero V, Astori G, Soldati G, Gola M, Surder D, Moccetti T: **A practical approach for the validation of sterility, endotoxin and potency testing of bone marrow mononucleated cells used in cardiac regeneration in compliance with good manufacturing practice.** *J Transl Med* 2009, **7**:78.
7. Joannides A, Fiore-Heriche C, Westmore K, Caldwell M, Compston A, Allen N, Chandran S: **Automated mechanical passaging: a novel and efficient method for human embryonic stem cell expansion.** *Stem Cells* 2006, **24**(2):230–235.
8. Kino-Oka M, Ogawa N, Umegaki R, Taya M: **Bioreactor design for successive culture of anchorage-dependent cells operated in an automated manner.** *Tissue Eng* 2005, **11**(3–4):535–545.
9. Terstegge S, Laufenberg I, Pochert J, Schenk S, Itskovitz-Eldor J, Endl E, Brustle O: **Automated maintenance of embryonic stem cell cultures.** *Biotechnol Bioeng* 2007, **96**(1):195–201.
10. Thomas RJ, Anderson D, Chandra A, Smith NM, Young LE, Williams D, Denning C: **Automated, scalable culture of human embryonic stem cells in feeder-free conditions.** *Biotechnol Bioeng* 2009, **102**(6):1636–1644.
11. Koike H, Kubota K, Sekine K, Takebe T, Ouchi R, Zheng YW, Ueno Y, Tanigawa N, Taniguchi H: **Establishment of automated culture system for murine induced pluripotent stem cells.** *BMC Biotechnol* 2012, **12**:81.
12. Thomas RJ, Chandra A, Liu Y, Hourd PC, Conway PP, Williams DJ: **Manufacture of a human mesenchymal stem cell population using an automated cell culture platform.** *Cytotechnology* 2007, **55**(1):31–39.
13. Hubbell JA, Palsson BO, Papoutsakis ET: **Preface: tissue engineering and cell therapies: II.** *Biotechnol Bioeng* 1994, **43**(8):683.
14. Thomas R, Chandra A, Hourd P, Williams D: **Cell culture automation and quality engineering: a necessary partnership to develop optimized manufacturing processes for cell-based therapies.** *J Assoc Lab Autom* 2008, **13**(3):152–158.
15. Thomas RJ, Hourd PC, Williams DJ: **Application of process quality engineering techniques to improve the understanding of the in vitro processing of stem cells for therapeutic use.** *J Biotechnol* 2008, **136**(3–4):148–155.
16. Takehara N, Ogata T, Nakata M, Kami D, Nakamura T, Matoba S, Gojo S, Sawada T, Yaku H, Matsubara H: *The ALCADIA (Autologous Human Cardiac-Derived Stem Cell to Treat Ischemic Cardiomyopathy) trial*, Circulation. PHILADELPHIA, PA: LIPPINCOTT WILLIAMS & WILKINS 530 WALNUT ST; 2012:19106–3621. USA: 2783–2783.
17. Toyoda M, Yamazaki-Inoue M, Itakura Y, Kuno A, Ogawa T, Yamada M, Akutsu H, Takahashi Y, Kanzaki S, Narimatsu H, *et al*: **Lectin microarray analysis of pluripotent and multipotent stem cells.** *Genes Cells* 2011, **16**(1):1–11.
18. Sharov AA, Dudekula DB, Ko MS: **A web-based tool for principal component and significance analysis of microarray data.** *Bioinformatics* 2005, **21**(10):2548–2549.
19. Ptaszek LM, Mansour M, Ruskin JN, Chien KR: **Towards regenerative therapy for cardiac disease.** *Lancet* 2012, **379**(9819):933–942.
20. Gojo S, Toyoda M, Umezawa A: **Tissue engineering and cell-based therapy toward integrated strategy with artificial organs.** *J Artif Organs* 2011, **14**(3):171–177.
21. Liu Y, Hourd P, Chandra A, Williams DJ: **Human cell culture process capability: a comparison of manual and automated production.** *J Tissue Eng Regen Med* 2010, **4**(1):45–54.
22. Kuroda Y, Kitada M, Wakao S, Nishikawa K, Tanimura Y, Makinoshima H, Goda M, Akashi H, Inutsuka A, Niwa A, *et al*: **Unique multipotent cells in adult human mesenchymal cell populations.** *Proc Natl Acad Sci USA* 2010, **107**(19):8639–8643.
23. Unger C, Skottman H, Blomberg P, Dilber MS, Hovatta O: **Good manufacturing practice and clinical-grade human embryonic stem cell lines.** *Human Mol Genet* 2008, **17**(R1):R48–R53.
24. Allport-Settle MJ: *Good Manufacturing Practice (GMP) Guidelines.* Raleigh: Pharmalogika; 2009.
25. Burger SR: **Current regulatory issues in cell and tissue therapy.** *Cytotherapy* 2003, **5**(4):289–298.
26. USP: *32-NF 27 Cell and gene therapy products.* United States Pharmacopeia, Rockville: Manufacturing of cell therapy products; 2008.
27. Niazi SK: *Sterile products, vol. 6.* London: Informa Healthcare Inc; 2009.
28. Takehara NOT, Nakata M, Kami D, Matoba NT, Gojo S, Sawada T, Yaku H, Matsubara H: *The ALCADIA (autologous Human Cardiac-derived Stem Cell To Treat Ischemic Cardiomyopathy) Trial*, Late Breaking Clinical Trial Application. Los Angeles: American Heart Association, Scientific Session; 2012.
29. Kuno A, Itakura Y, Toyoda M, Takahashi Y, Yamada M, Umezawa A, Hirabayashi J: **Development of a data-mining system for differential**

profiling of cell glycoproteins based on lectin microarray. *J Proteom Bioinfo* 2008, 1(2):5.

30. Itakura Y, Kimura M, Gojo S, Toyoda M, Kami D, Motomura N, Umezawa A, Kyo S, Ono M: **Glycan profiling using a lectin microarray is a novel validation tool for monitoring the damage to freeze-thawed cells.** *Low Temp Med* 2011, **37**:7.

doi:10.1186/1472-6750-13-102
Cite this article as: Kami *et al.*: Large-scale cell production of stem cells for clinical application using the automated cell processing machine. *BMC Biotechnology* 2013 **13**:102.

Submit your next manuscript to BioMed Central and take full advantage of:

- Convenient online submission
- Thorough peer review
- No space constraints or color figure charges
- Immediate publication on acceptance
- Inclusion in PubMed, CAS, Scopus and Google Scholar
- Research which is freely available for redistribution

Submit your manuscript at
www.biomedcentral.com/submit

BioMed Central

HERPESVIRIDAE

RESEARCH Open Access

Human cytomegalovirus induces apoptosis in neural stem/progenitor cells derived from induced pluripotent stem cells by generating mitochondrial dysfunction and endoplasmic reticulum stress

Hiroyuki Nakamura[1*], Huanan Liao[1], Kahori Minami[2], Masashi Toyoda[2], Hidenori Akutsu[2], Yoshitaka Miyagawa[3], Hajime Okita[3], Nobutaka Kiyokawa[3], Akihiro Umezawa[2], Ken-Ichi Imadome[1], Naoki Inoue[4] and Shigeyoshi Fujiwara[1]

Abstract

Background: Congenital human cytomegalovirus (HCMV) infection, a leading cause of birth defects, is most often manifested as neurological disorders. The pathogenesis of HCMV-induced neurological disorders is, however, largely unresolved, primarily because of limited availability of model systems to analyze the effects of HCMV infection on neural cells.

Methods: An induced pluripotent stem cell (iPSC) line was established from the human fibroblast line MRC5 by introducing the Yamanaka's four factors and then induced to differentiate into neural stem/progenitor cells (NSPCs) by dual inhibition of the SMAD signaling pathway using Noggin and SB-431542.

Results: iPSC-derived NSPCs (NSPC/iPSCs) were susceptible to HCMV infection and allowed the expression of both early and late viral gene products. HCMV-infected NSPC/iPSCs underwent apoptosis with the activation of caspase-3 and −9 as well as positive staining by the terminal deoxynucleotidyl transferase-mediated dUTP nick-end labeling (TUNEL). Cytochrome c release from mitochondria to cytosol was observed in these cells, indicating the involvement of mitochondrial dysfunction in their apoptosis. In addition, phosphorylation of proteins involved in the unfolded protein response (UPR), such as PKR-like eukaryotic initiation factor 2a kinase (PERK), c-Jun NH2-terminal kinase (JNK), inositol-requiring enzyme 1 (IRE1), and the alpha subunit of eukaryotic initiation factor 2 (eIF2α) was observed in HCMV-infected NSPC/iPSCs. These results, coupled with the finding of increased expression of mRNA encoding the C/EBP-homologous protein (CHOP) and the detection of a spliced form of X-box binding protein 1 (XBP1) mRNA, suggest that endoplasmic reticulum (ER) stress is also involved in HCMV-induced apoptosis of these cells.

Conclusions: iPSC-derived NSPCs are thought to be a useful model to study HCMV neuropathogenesis and to analyze the mechanisms of HCMV-induced apoptosis in neural cells.

Keywords: Human cytomegalovirus, iPS cells, Neural stem/progenitor cells, Apoptosis, ER stress

* Correspondence: nakamura-hry@ncchd.go.jp
[1]Department of Infectious Diseases, National Research Institute for Child Health and Development, 2-10-1 Okura, Setagaya-ku, Tokyo 157-8535, Japan
Full list of author information is available at the end of the article

BioMed Central

© 2013 Nakamura et al.; licensee BioMed Central Ltd. This is an open access article distributed under the terms of the Creative Commons Attribution License (http://creativecommons.org/licenses/by/2.0), which permits unrestricted use, distribution, and reproduction in any medium, provided the original work is properly cited.

Background

Congenital cytomegalovirus (CMV) infection is a major cause of birth defects resulting mainly from primary CMV infection during pregnancy. At birth, approximately 5 to 10% of congenitally infected newborns are estimated to be symptomatic exhibiting multi-organ disorders including neurological defects such as mental retardation, sensorineural hearing loss, and microencephaly [1,2]. A latest study showed that if laboratory findings including those from magnetic resonance imaging (MRI) images of the brain are considered, up to 30% of congenitally infected newborns exhibit some abnormal signs [3]. Sixty to 90% of congenitally infected children who are symptomatic at birth, and 10 to 15% of those who are asymptomatic at birth develop one or more long-term sequelae. Although CMV infects a wide variety of cell types, infection of the nervous system gives most serious and long-lasting damages to the host.

As a part of understanding the HCMV neuropathogenesis, it is important to scrutinize the cellular response to CMV infection in neural cells. Some human neural cell lines can be infected with HCMV with different permissiveness to HCMV gene expression and replication [4-7]. A recent study has shown that neural progenitor cells isolated from developing human brain tissues are susceptible to CMV infection and undergo apoptosis following infection [8,9]. However, the amount of neural cells obtainable from human brain tissues is limited.

Pluripotent stem cells, including embryonic stem cells (ESCs) and induced pluripotent stem cells (iPSCs), are characterized by the ability to differentiate into tissues derived from any of the three embryonic germ layers. Recent advances in the method to induce efficient differentiation of either ESCs or iPSCs into specific cell lineages offer an opportunity to establish model systems for viral infections of various cell types, including neural cells. Furthermore, differentiated cells derived from pluripotent stem cells are obtainable in potentially unlimited amounts. Previous works revealed that while mouse ESCs are not susceptible to murine CMV (MCMV), NSPCs that are differentiated from them are susceptible and their proliferation and differentiation are suppressed by MCMV [10-13]. Experiments with human ESCs are, however, complicated with ethical problems.

In this study, to analyze the pathological effects of HCMV on neural cells, we prepared NSPCs from human iPSCs and examined whether NSPCs are susceptible to HCMV infection. The results indicated that NSPCs are susceptible to HCMV infection and undergo apoptosis caused by mitochondrial dysfunction and endoplasmic reticulum (ER) stress.

Methods

Cells and viruses

The human fetal lung fibroblast MRC5 was grown in Dulbecco's modified Eagle's medium (DMEM) supplemented with 10% fetal bovine serum (FBS; Invitrogen, Carlsbad, CA). The human foreskin fibroblast cell line hTERT-BJ1 immortalized with the human telomerase reverse transcriptase (Clontech, Palo Alto, CA) was grown in a medium consisting of 4 parts of DMEM and 1 part of medium 199 (Sigma) supplemented with 10% FBS, 1 mM sodium pyruvate (Sigma), and 2 mM glutamine (Invitrogen). HCMV laboratory strain Towne (ATCC VR-977) was propagated in hTERT-BJ1 cells. The human iPSC line MRC-iPS-25 that was established from MRC5 by retroviral vector-mediated transduction of the c-Myc, Oct-4, Klf4, and Sox2 genes [14,15] were cultured on mitomycin C-treated mouse embryonic fibroblasts (MEFs) in an iPSC medium consisting of Knockout DMEM/F12 (Invitrogen) supplemented with non-essential amino acids (0.1 mM, Invitrogen), glutamax I (1 mM, Invitrogen), 20% Knockout Serum Replacement (Invitrogen), β-mercaptoethanol (55 μM, Invitrogen) and basic fibroblast growth factor (10 ng/mL; Peprotech, Rocky Hill, NJ).

Induced differentiation on iPSCs into neural stem cells

MRC-iPSC-25 cells cultured under feeder-free conditions were induced to differentiate into neural stem/progenitor cells (NSPCs) by the method of dual inhibition of the SMAD signaling pathway described previously [16]. In brief, feeder-free iPSCs were treated with the mTeSR1 medium (StemCell Technologies, Vancouver, BC, Canada) containing Y27632 (Wako Pure Chemicals, Osaka, Japan) and maintained with a daily medium change for 4 days. Then the medium was replaced with iPSC medium supplemented with SB431542 (10 nM, Wako Pure Chemicals) and Noggin (500 ng/ml, Wako Pure Chemicals). This date was designated day 0. On day 2, culture medium was replaced with a medium consisting of 3 parts of iPSC medium and 1 part of N2 medium (Knockout DMEM/F12 containing 1× N2 supplement) supplemented with SB431542 (10 nM) and Noggin (500 ng/ml). On day 4, culture medium was replaced with a medium consisting of 1 part of iPSC medium and 1 part of N2 medium supplemented with SB431542 (10 nM) and Noggin (500 ng/ml). On day 6, cells were expanded in StemPro NSC SFM (Invitrogen). MRC-iPSC-25 cells cultured under feeder-free conditions and NSPC/iPSCs were infected with the Towne strain HCMV at a multiplicity of infection (MOI) of 1 plaque forming unit (PFU) per cell. To detect infectious virions produced from HCMV-infected NSPC/iPSCs, supernatant was collected and replaced with fresh medium every two days after infection. hTERT-BJ1 cells were inoculated with the supernatant and examined by IFA for expression of IE1/IE2.

Antibodies

Antibodies used were as follows: rabbit anti-Sox2, rabbit anti-Nanog, rabbit anti-Oct-4, rabbit anti-cleaved caspase-

3, rabbit anti-cleaved caspase-9, rabbit anti-phospho-eIF2α (Ser51), rabbit anti-phospho-PERK (Thr980), and rabbit anti-phospho-SAPK/JNK (Thr183/Tyr185)(Cell Signaling Technology, Beverly, MA); mouse anti-CMV IE1/IE2, rabbit anti-Musashi-1, and rabbit anti-cytochrome c (Millipore, Temecula, CA); rabbit anti-Nestin and mouse anti-α-tubulin (Sigma-Aldrich, St. Louis, MO); rabbit anti-Pax6 (Covance, Princeton, NJ), mouse anti-CMV gB (Abcam, Cambridge, MA); mouse anti-pp65 (Virusys Corporation, Sykesville, MD); rabbit anti-phosphorylated IRE1α (Pierce/Thermo Scientific, Rockford, IL); Alexa Fluor 488-conjugated goat anti-mouse IgG and Alexa Fluor 594-conjugated goat anti-rabbit IgG (Molecular Probes, Eugene, OR); horseradish peroxidase-conjugated donkey anti-rabbit IgG and horseradish peroxidase-conjugated sheep anti-mouse IgG (GE Healthcare, UK).

Immunofluorescence microscopy and immunoblot analysis

Cells were fixed with 4% parafolmaldehyde in PBS (Wako chemicals) at room temperature (RT) for 15 min. After fixation, cells were treated with 1.0% Triton X-100 in PBS for 15 min at RT and blocked with 10% goat serum in PBS for 30 min. Cells were incubated with the primary antibody at 4°C overnight, followed by washing in PBS and incubation with the corresponding secondary antibody at 37°C for 1 h. Nuclei were stained with DAPI. For the assessment of cell death, terminal deoxynucleotidyl transferase (TdT)-mediated dUTP nick-end labeling (TUNEL) assay was performed according to the manufacturer's instructions (Roche). Immunoblot analyses were performed as described previously [17].

Reverse transcriptase (RT)-PCR and real-time quantitative RT-PCR

Total RNA was isolated from mock- or HCMV-infected cells using TRIzol reagent (Invitrogen). Reverse transcription was performed on each RNA sample (5 μg) using SuperScript III First-Strand Synthesis System for RT-PCR (Invitrogen). Primer sequences are shown in Table 1. RT-PCR products were resolved by electrophoresis on 2% agarose gel and then visualized by ultraviolet illumination after ethidium bromide staining. Real-time quantitative RT-PCR was performed using TaqMan™ Universal Master Mix II with UNG (Applied Biosystems) on a StepOne Plus PCR System (Applied Biosystems). Amplifications were achieved in a final volume of 25 μl containing TaqMan probes labeled with FAM on the 5'-end and MGB on the 3'-end. The primers and probes for *UL136* were: forward primer, 5'-GGCCGTTGAACGGAGCTAT-3' and reverse primer, 5'-CCATTTCCACCGTGTCGAA-3', and TaqMan probe, 5'-FAM-TACTACGGCAGCGGCT-MGB-3'. The forward and reverse primers and reporter probes for HCMV *IE1*, *UL89*, and Human *G6PD* were described previously [18].

Table 1 List of primer sequences for RT-PCR

Gene	Forward primer	Reverse primer
IE1*	ATGGAGTCCTCTGCCAAGAG	ATTCTATGCCGCACCATGTCC
IE2*	ATGGAGTCCTCTGCCAAGAG	CTGAGACTTGTTCCTCAGGTCCTG
vIL-10*	ATGCTGTCGGTGATGGTCTCTTCC	CTTTCTCGAGTGCAGATACTCTTCG
UL36*	GACCTACGGGACACGCTGATG	TGTGGAAGTGGTCGCAGTGAC
UL38	GACTACGACCACGCATAGCA	GGGAACAGAGCGTTCCAATA
pp65	CGCAACCTGGTGCCCATGG	CGTTTGGGTTGCGCAGCGGG
Nanog*	GCTTGCCTTGCTTTGAAGCA	TTCTTGACCGGGACCTTGTC
Oct-4	GAGCAAAACCCGGAGGAGT	TTCTCTTTCGGGCCTGCAC
Sox1	GCGGAAAGCGTTTTCTTTG	TAATCTGACTTCTCCTCCC
Sox2	ATGCACCGCTACGACGTGA	CTTTTGCACCCCTCCCATTT
Pax6*	AACAGACACAGCCCTCACAAACA	CGGGAACTTGAACTGGAACTGAC
Nestin*	CAGCGTTGGAACAGAGGTTGG	TGGCACAGGTGTCTCAAGGGTAG
MAP2*	CCACCTGAGATTAAGGATCA	GGCTTACTTTGCTTCTCTGA
GFAP*	GTACCAGGACCTGCTCAAT	CAACTATCCTGCTTCTGCTC
OSP*	ACTGCTGCTGACTGTTCTTC	GTAGAAACGGTTTTCACCAA
XBP1*	CCTTGTAGTTGAGAACCAGG	GGGGCTTGGTATATATGTGG
CHOP*	TGGAAGCCTGGTATGAGGAC	TCACCATTCGGTCAATCAGA
β-actin*	ACCATGGATGATGATATCGC	TCATTGTAGAAGGTGTGGTG
GAPDH*	CCACCCATGGCAAATTCCATGGCA	TCTAGACGGCAGGTCAGGTCCACC

Asterisks (*) indicate that amplified fragments contain splicing junctions. Amplified fragments for UL38, pp65, Oct-4, Sox1, and Sox2 did not contain splicing junctions, and therefore control experiments without reverse transcriptase confirmed the RNA origin of the PCR products.

Results

Preparation of human iPSC-derived neural stem/progenitor cells

Figure 1A demonstrates that MRC-iPS-25 cells have a typical iPSC colony morphology. The expression of pluripotency markers of iPSCs such as Nanog and Oct-4 in MRC-iPS-25 cells was confirmed by indirect immunofluorescence assay (IFA) (Figure 1B). The HCMV-encoded proteins IE1/IE2 were not detected in MRC-iPS-25 cells following inoculation with the virus, indicating that MRC-iPS-25 cells are either not susceptible to HCMV infection or do not support expression of the IE genes (Figure 1B).

NSPC/iPSCs prepared by induced differentiation of MRC-iPS-25 cells proliferated in a monolayer and displayed a rounded, immature neural morphology (Figure 1A). IFA (Figure 1C) showed that NSPC/iPSCs expressed the NSC markers Nestin, Sox2, and Pax6, indicating that NSPC/iPSCs have the authentic NSPC phenotype.

In vitro HCMV infection of iPSC-derived NSPCs

To examine the susceptibility of NSPC/iPSCs to HCMV infection, these cells were inoculated in vitro with the HCMV Towne strain at an MOI of 1 PFU per cell (Figure 2A). On the second day post-infection (dpi), NSPC/iPSCs started to show morphological changes including increased cell volume and cell fusion, and the number of cells with these

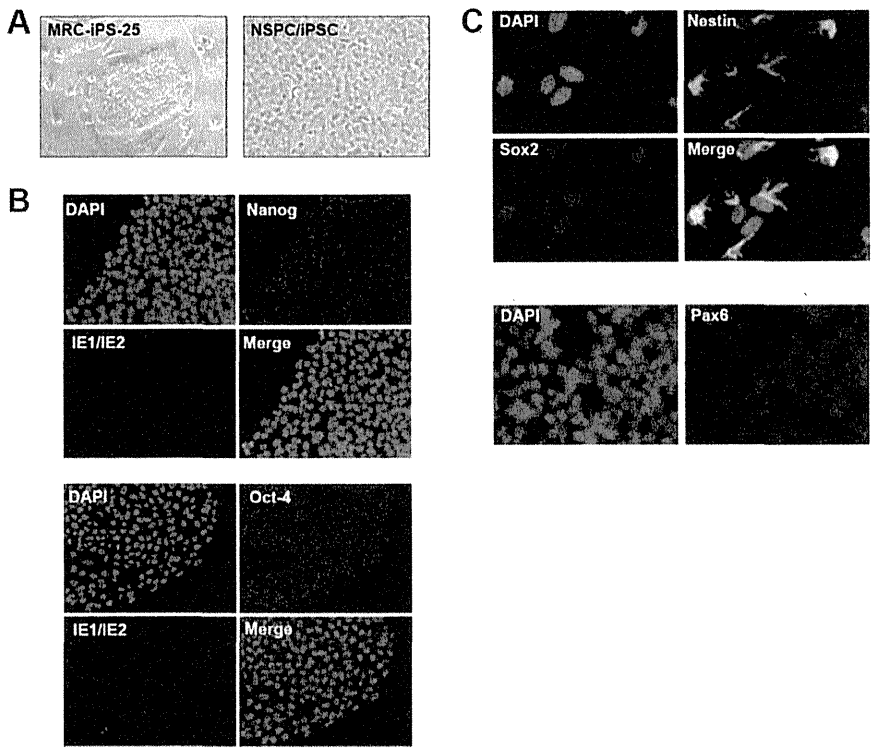

Figure 1 Differentiation of MRC-iPS-25 cells to neural stem/progenitor cells. (A) Phase-contrast images of MRC-iPS-25 cells cultured on a feeder layer of MEFs (left) and NSPC/iPSCs (right). **(B)** Immunofluorescence analysis of Towne-infected MRC-iPS-25 cells cultured under feeder-free conditions at 2 dpi stained with primary antibodies for pluripotent markers (Nanog or Oct-4) and HCMV IE1/IE2 proteins. Antigen proteins were detected with Alexa Fluor 488-conjugated goat anti-mouse IgG or Alexa Fluor 594-conjugated goat anti-rabbit IgG antibody. Nuclei were stained with DAPI. **(C)** Immunofluorescence analysis of NSPC markers Nestin, Sox2, and Pax6 in NSPC/iPSCs. NSPC/iPSCs were fixed and reacted with anti-Nestin (green), anti-Sox2 (red), and anti-Pax6 (red) antibodies, followed by detection with secondary antibodies. Immunofluorescence signals were obtained using a fluorescence microscope IX71. *Representative results from three independent experiments are shown.*

changes increased until 7 dpi (Figure 2A). To examine whether NSPC/iPSCs were capable of supporting HCMV gene expression, total RNA extracted from the infected NSPC/iPSCs was analyzed by RT-PCR. As shown in Figure 2B, mRNAs encoding IE1, IE2, vIL-10, and pp65 as well as those encoding HCMV anti-apoptotic proteins, such as UL36 and UL38, were detected. The kinetics of HCMV gene expression was analyzed by quantitative real-time RT-PCR (Figure 2C). IE1 mRNA was detected first on 1 dpi and increased steadily until 5 dpi. mRNAs for UL89 and UL136 were detected somewhat later and increased gradually until 7 dpi. The results showed the NSPC/iPSCs are susceptible to HCMV infection and allow the expression of several viral genes of both early and late functions.

Expression of HCMV genes in NSPC/iPSCs was evaluated at the protein level by immunoblot analysis on day 1, 2, 5, and 7 following HCMV infection. As shown in Figure 2D, the immediate-early protein IE1 was first detected at 1 dpi and its level increased until 5 dpi. Another immediate-early protein IE2 was detected a little later, becoming visible at 5 dpi. The expression of the HCMV lower matrix protein pp65 (ppUL83), already visible at 1 dpi, was markedly elevated at 5 and 7 dpi. The HCMV envelope glycoprotein B (gB; UL55) was detected at 5 to 7 dpi. Thus the expression of HCMV proteins of both immediate-early and late functions was demonstrated in NSPC/iPSCs.

We next examined the expression of cellular mRNAs encoding the pluripotency and neural differentiation markers (Figure 2E). Expression of the iPSC markers Nanog and Oct-4 remained at low levels following infection with HCMV, although that of Nanog tapered. While expression of the NSPC markers Sox2 and Pax6 were kept at high levels following HCMV infection, that of another NSPC marker Nestin was markedly suppressed at 7 dpi. In addition, expression of the neuronal marker microtubule-associated protein 2 (MAP2), the astrocyte marker glial fibrillary acidic protein (GFAP), and the oligodendrocyte marker oligodendrocyte-specific protein (OSP) was detected at low levels. Interestingly, Sox1, a marker specific to the neuroectodermal lineages [19], was markedly upregulated following infection with HCMV. Expression of the NSPC markers was evaluated

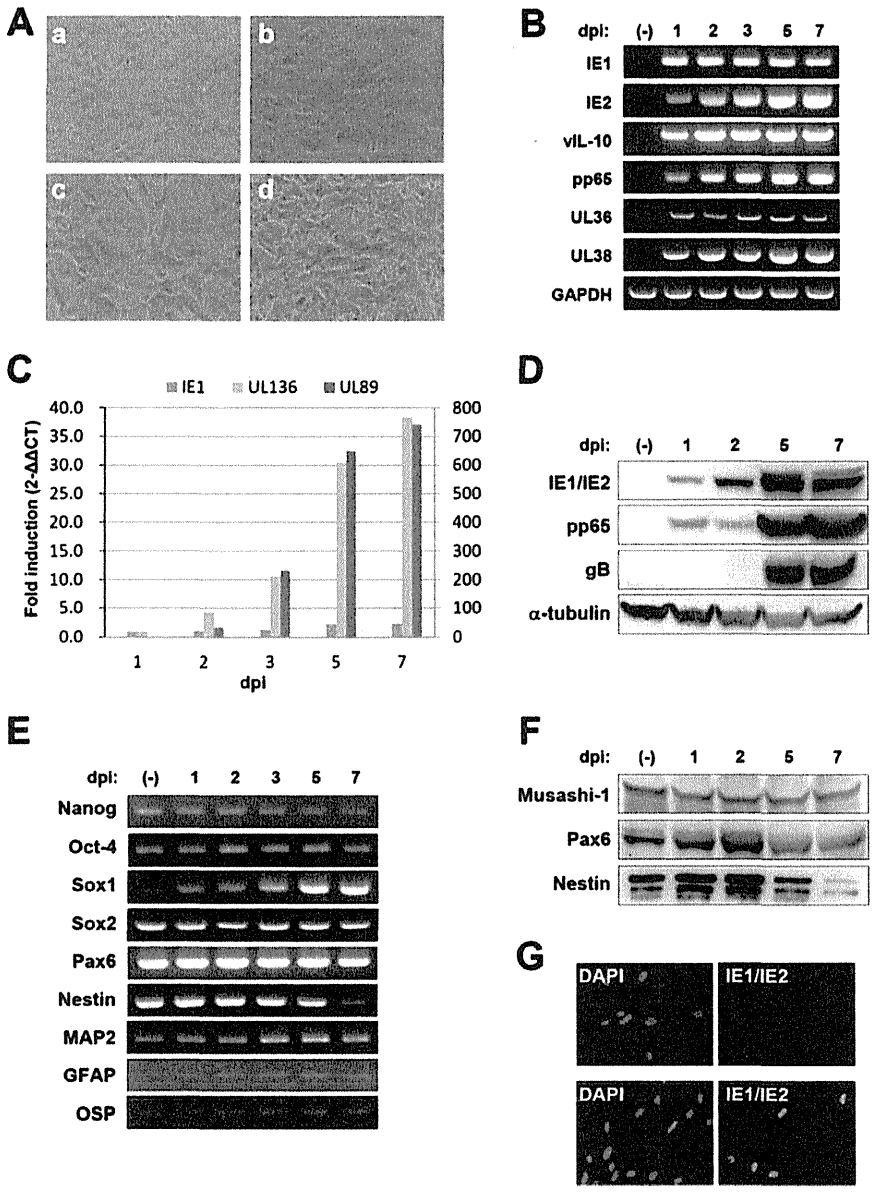

Figure 2 Analysis on the expression of viral and cellular gene products in NSPC/iPSCs. **(A)** *Morphological changes of Towne-infected* NSPC/iPSCs were observed under the inverted microscope before infection **(a)**, 2 dpi **(b)**, 5 dpi **(c)**, and 7 dpi **(d)**. **(B)** RT-PCR analysis of HCMV-encoding gene expression. Total RNAs isolated from NSPC/iPSCs harvested before (–) HCMV infection or at 1, 2, 3, 5, and 7 dpi with HCMV Towne strain were subjected to RT-PCR assays. GAPDH gene expression was assayed for the control. **(C)** The kinetics of mRNA expression for IE1, UL89, and UL136 in Towne-infected NSPC/iPSCs was examined by real-time quantitative RT-PCR assay. The mRNA expression was normalized to that of G6PDH gene. Real-time PCR data was analyzed by the 2-ΔΔCT method. The fold induction was calculated as the ratio of mRNA levels detected at each time point to that detected at 1 dpi. The y-axis represents fold induction of IE1 and UL136 mRNA (left y-axis) and UL89 mRNA (right y-axis). **(D)** Immunoblot analysis of HCMV protein expression in HCMV-infected NSPC/iPSCs. Whole-cell lysates of NSPC/iPSCs harvested before (–) HCMV infection or at 1, 2, 5, and 7 dpi with HCMV Towne strain were separated by SDS-PAGE and analyzed by immunoblotting with antibodies against IE1/IE2, pp65, gB, and α-tubulin. **(E)** RT-PCR analysis of pluripotency and neural differentiation marker gene expression in HCMV-infected NSPC/iPSCs. **(F)** Immunoblot analysis of neural differentiation marker protein expression in HCMV-infected NSPC/iPSCs. Whole-cell lysates of NSPC/iPSCs were analyzed by immunoblotting with antibodies against Musashi-1, Pax6, and Nestin. **(G)** hTERT-BJ1 cells inoculated with culture supernatant collected from mock-infected NSPC/iPSCs (upper panel) or Towne HCMV-infected NSPC/iPSCs (lower panel) at 8 dpi were subjected to immunofluorescence test with anti-IE1/IE2 antibody (green). Nuclei were stained with DAPI. Representative results from two independent experiments are shown.

also at the protein level by immunoblot analysis on 1, 2, 5, and 7 dpi (Figure 2F). In accordance with the results with RT-PCR, expression of Pax6 and Nestin was confirmed, and that of Nestin was found markedly decreased 7 dpi. Another NSPC marker Musashi-1 was also detected. To examine whether HCMV-infected NSPC/iPSCs produce infectious virions, culture supernatants collected from Towne HCMV-infected NSPC/iPSCs were inoculated to hTERT-BJ1 cells. Inoculated cells expressed IE1/IE2 indicating that infectious virions were produced from HCMV-infected NSPC/iPSCs (Figure 2G). The supernatant contained 30 PFU/mL of HCMV at 4, 6, 8 dpi, while no plaque forming virus was detected at 2 dpi.

HCMV infection induces apoptosis in iPSC-derived NSPCs

To examine whether HCMV infection in NSPC/iPSCs induces apoptotic responses, we performed the TUNEL assay combined with IFA using an antibody specific to HCMV gB. As shown in Figure 3A, NSPC/iPSCs expressing gB was positive for TUNEL staining and those without gB expression was consistently negative. We also performed IFA to analyze the activation status of caspases using antibodies specific to the activated forms of caspase-3 and caspase-9. The results show that the activated forms of caspase-3 and caspase-9 were specifically detected in more than 80% of HCMV-infected NSPC/iPSCs expressing IE1/IE2 proteins (Figure 3B and 3C), but not in mock-infected NSPC/iPSCs (Figure 3E). To see whether mitochondrial dysfunction is involved in the activation of caspase 9, intracellular distribution of cytochrome c was analyzed in HCMV-infected cells by IFA. As shown in Figure 3D and 3E, strong signals of cytochrome c were detected in the cytosol of cells expressing IE1/IE2 proteins, while only faint signals of cytochrome c were detected in cells not expressing IE1/IE2 proteins or in mock-infected cells. These results indicate that HCMV infection of NSPC/iPSCs activated apoptotic responses involving release of mitochondrial cytochrome c and serial activation of caspases.

Unfolded protein response in HCMV-infected NSPC/iPSCs

The unfolded protein response (UPR), induced by the accumulation of improperly folded proteins within the ER lumen (ER stress), is associated with multiple cellular responses such as neurodegeneration and apoptosis. ER stress sensor molecules, such as PKR-like eukaryotic initiation factor 2a kinase (PERK) and inositol-requiring enzyme 1 (IRE1), are activated on UPR and engage downstream signaling pathways. To examine whether the caspase-9 activation in HCMV-infected NSPC/iPSCs (Figure 3C) is associated with UPR, we analyzed phosphorylation status of IRE1α and its downstream target c-Jun NH2-terminal kinase (JNK) in immunofluorescence assays. Both IRE1α and JNK were specifically phosphorylated in HCMV-infected NSPC/iPSCs (Figure 4A and 4B), but not in mock-infected NSPC/iPSCs (Figure 4C). In concordance with the previous reports that activated IRE1α catalyzes the non-conventional splicing of the mRNA encoding X-box binding protein 1 (XBP1) [20,21], the spliced XBP1 mRNA increased gradually after HCMV infection in NSPC/iPSCs (Figure 4D). We also analyzed phosphorylation status of another sensor molecule PERK, an ER-associated serine/threonine protein kinase, and its downstream target the alpha subunit of eukaryotic initiation factor 2 (eIF2α). Phosphorylated forms of PERK and eIF2α were specifically detected in HCMV-infected NSPC/iPSCs (Figure 4E and 4F), but not in mock-infected NSPC/iPSCs (Figure 4G). The transcription factor activating transcription factor 4 (ATF4), that is preferentially translated on activation of PERK, induces the expression of C/EBP-homologous protein (CHOP/GADD153), a transcription factor with proapoptotic functions [22]. In accordance with these previous findings, the mRNA level of CHOP increased gradually after HCMV infection in NSPC/iPSCs (Figure 4H). These results suggest that UPR is involved in the activation of caspase cascade leading to apoptosis in HCMV-infected NSPC/iPSCs.

Discussion

Important findings in this study are as follows: i) NSPC/iPSCs derived from MRC-iPS-25 cells were susceptible to HCMV infection and allow the expression of viral gene products of both early and late functions and production of infectious virions. In contrast, MRC-iPS-25 cells before induction of differentiation was either resistant to HCMV or did not support the expression of HCMV immediate-early genes; ii) the HCMV-infected NSPCs undergo apoptosis; and iii) the mechanism of the apoptosis included cytochrome c release from mitochondria to cytosol and activation of UPR-related signaling pathways.

Neuropathogenesis of HCMV infection has been studied mainly with neural cells isolated from human brain. These studies demonstrated that HCMV can infect human neural precursor cells (NPCs) isolated from fetal brains and interfere with their differentiation. Luo et al. [23] showed that HCMV infection in primary NPCs reduced the expression of Nestin, suggesting that HCMV affects the differentiation potential of NPCs. Similar results were also obtained from experiments with mouse NSCs infected with MCMV [10,13,24]. Those previous findings obtained from experiments with primary cultures of brain-derived neural cells were thus mostly reproduced in our experiments using NSPC/iPSCs. In addition, similar to the results of Odeberg et al. [8] that used NPCs derived from human brain, we also demonstrated that HCMV infection induced apoptosis in NSPC/iPSCs obtained from iPSCs. It is thus supposed that neural cells differentiated from iPSCs are a useful

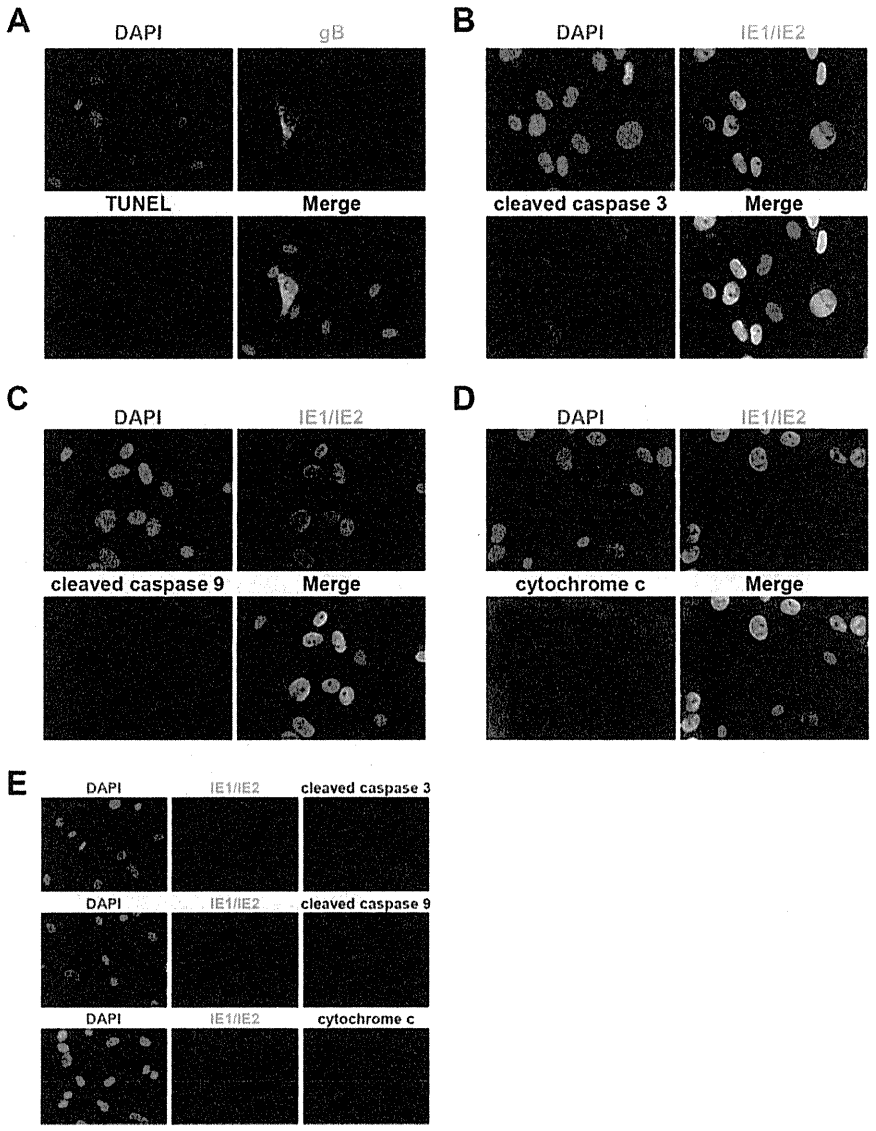

Figure 3 HCMV-induced apoptosis of NSPC/iPSCs. (A) Towne-infected NSPC/iPSCs at 6 dpi were subjected to TUNEL assay followed by immunofluorescence test with an anti-gB antibody. TUNEL-positive nuclei were stained in red. The anti-gB antibody was detected with Alexa Fluor 488-conjugated goat anti-mouse IgG antibody (green). Nuclei were stained with DAPI. **(B-D)** Towne-infected NSPC/iPSCs at 3 dpi were subjected to immunofluorescence test with anti-IE1/IE2 antibody in combination with anti-cleaved caspase 3 **(B)**, anti-cleaved caspase 9 **(C)**, or anti-cytochrome c **(D)** antibody. Alexa Fluor 488-conjugated goat anti-mouse IgG (green) or Alexa Fluor 594-conjugated goat anti-rabbit IgG antibody (red) was used as a secondary antibody. Nuclei were stained with DAPI. **(E)** Mock-infected NSPC/iPSCs were subjected to immunofluorescence test with anti-IE1/IE2 antibody in combination with anti-cleaved caspase 3 (upper panel), anti-cleaved caspase 9 (middle panel), or anti-cytochrome c (lower panel) antibody. Nuclei were stained with DAPI. Representative results from two independent experiments are shown.

model to investigate neural pathogenesis of HCMV. In the human brain, NSCs are predominantly found in the subventricular region where CMV infections preferentially occur [25,26]. Analysis on the effects of HCMV infection on NSPCs can be therefore particularly relevant.

In the regulation of cellular apoptotic responses, mitochondrial dysfunction and ER stress are involved in the activation of the initiator caspase caspase-9 that functions as a trigger of cascade protease reactions leading to cell death. The finding of cytochrome c release from mitochondria to cytoplasm in HCMV-infected NSPC/iPSCs indicates that mitochondrial dysfunction is involved in the activation of caspase-9 in these cells. In addition, the demonstration of phosphorylated forms of proteins involved in UPR, including PERK, JNK, IRE1α, eIF2α, as well as that of unconventional splicing of

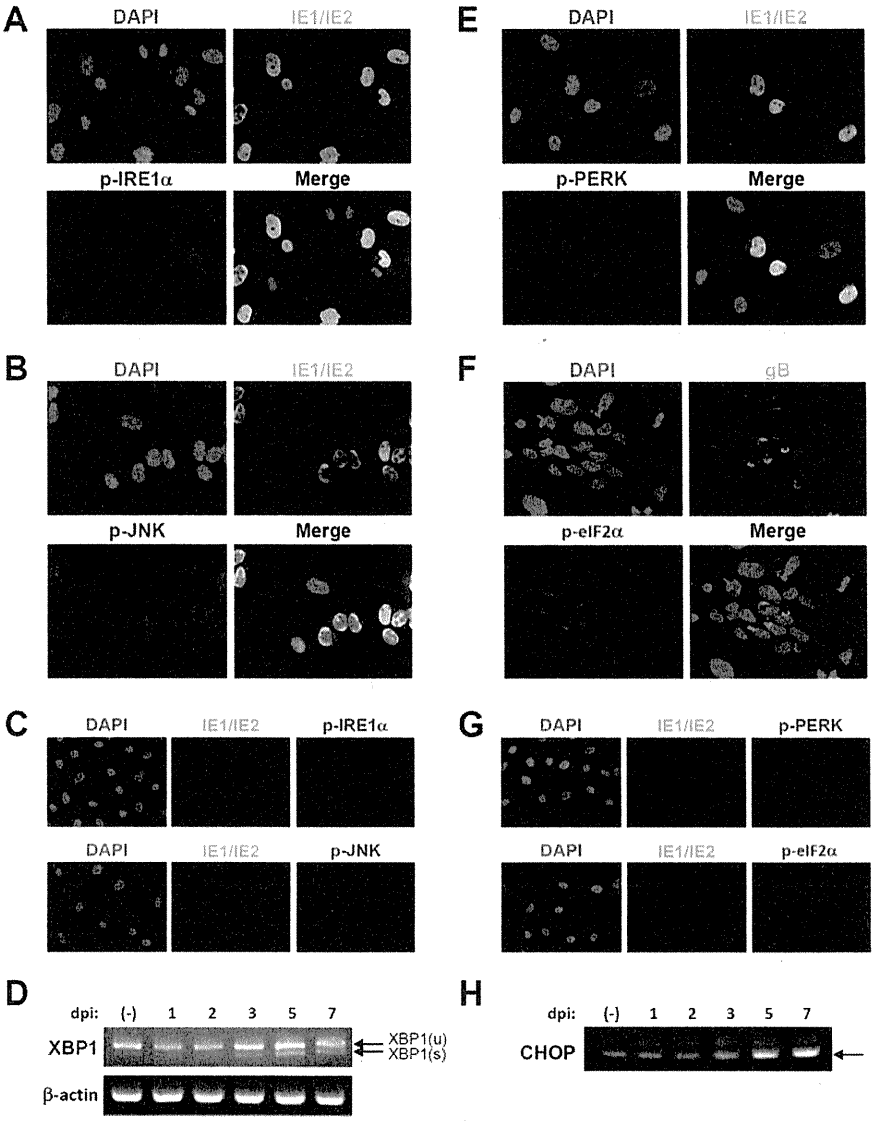

Figure 4 HCMV-induced UPR in NSPC/iPSCs. (A and B) Towne-infected NSPC/iPSCs at 3 dpi were subjected to immunofluorescence test with anti-IE1/IE2 antibody in combination with anti-phosphorylated IRE1α **(A)** or anti-phosphorylated JNK **(B)** antibody. Nuclei were stained with DAPI. **(C)** Mock-infected NSPC/iPSCs were subjected to immunofluorescence test with anti-IE1/IE2 antibody in combination with anti-phosphorylated IRE1α (upper panel) or anti-phosphorylated JNK (lower panel) antibody. Nuclei were stained with DAPI. **(D)** Detection of XBP1 (u, unspliced) and XBP1 (s, spliced) mRNAs in HCMV-infected NSPC/iPSCs. Total RNAs isolated from NSPC/iPSCs harvested before (–) HCMV infection or at 1, 2, 3, 5, and 7 dpi with HCMV Towne strain were subjected to RT-PCR assays. Amplified DNA fragments were separated in a 2% agarose gel and then photographed. Beta-actin gene expression was assayed for the control. **(E and F)** Towne-infected NSPC/iPSCs at 3 dpi were subjected to immunofluorescence test with anti-IE1/IE2 antibody in combination with anti-phosphorylated PERK **(E)** or anti-gB antibody in combination with anti-phosphorylated eIF2α **(F)** antibody. **(G)** Mock-infected NSPC/iPSCs were subjected to immunofluorescence test with anti-IE1/IE2 antibody in combination with anti-phosphorylated PERK (upper panel) or anti-phosphorylated eIF2α (lower panel) antibody. Nuclei were stained with DAPI. **(H)** Expression of CHOP mRNA in HCMV-infected NSPC/iPSCs. Total RNAs isolated from NSPC/iPSCs harvested before (–) HCMV infection or at 1, 2, 3, 5, and 7 dpi with HCMV Towne strain were subjected to RT-PCR assays. Representative results from three independent experiments are shown.

XBP1 mRNA and up-regulation of CHOP, indicate that ER stress also plays a role in HCMV-induced apoptosis of NSPC/iPSCs. These results are in accordance with the work reported by Isler et al. [27] who demonstrated that HCMV-induced UPR in human foreskin fibroblasts. HCMV is known to encode anti-apoptotic proteins such as viral inhibitor of caspase-8-induced apoptosis (vICA) encoded by UL36 [28], and pUL38 which protects against ER stress-induced cell death by modulating the UPR pathway [29]. Our RT-PCR analysis demonstrated

that such viral anti-apoptotic genes were expressed at transcription level in NSPC/iPSCs following HCMV infection (Figure 2B). Although these viral anti-apoptotic proteins did not block apoptosis of NSPC/iPSCs, they might have contributed for efficient viral replication by delaying apoptosis.

iPSCs are expected to be an innovative tool for not only regenerative medicine but also for the elucidation of pathogenesis of various diseases. Recent studies have shown that human iPSCs can be used also for modeling viral infection. Hepatocyte-like cells derived from human iPSCs were shown to be susceptible to hepatitis virus C infection and supported its replication [30,31]. Sensory neurons derived from human iPSCs were reported to be susceptible to infection with both varicella-zoster virus and herpes simplex virus [32]. While the present work was in progress, D'Aiuto and others reported on the preparation of an iPSC-derived model of HCMV infection in neural precursor cells [33]. Whereas our data described in the present study is largely consistent with their results, we further analyzed the mechanisms of apoptosis induction and elucidated the involvement of mitochondrial dysfunction and ER stress.

In conclusion, human NSPCs derived from iPSCs can be a useful model to study HCMV neuropathogenesis associated with congenital HCMV infection. They can be particularly valuable in analyzing the mechanisms of HCMV-induced apoptosis in neural cells.

Abbreviations

HCMV: Human cytomegalovirus; iPSC: Induced pluripotent stem cell; ESC: Embryonic stem cell; NSPC: Neural stem/progenitor cell; TUNEL: Terminal deoxynucleotidyl transferase-mediated dUTP nick-end labeling; UPR: Unfolded protein response; ER: Endoplasmic reticulum; PERK: PKR-like eukaryotic initiation factor 2a kinase; JNK: c-Jun NH2-terminal kinase; IRE1: Inositol-requiring enzyme 1; eIF2α: Alpha subunit of eukaryotic initiation factor 2; CHOP: C/EBP-homologous protein; XBP1: X-box binding protein 1; IFA: Indirect immunofluorescence assay; Dpi: Days post-infection; MAP2: Microtubule-associated protein 2; GFAP: Glial fibrillary acidic protein; OSP: Oligodendrocyte-specific protein; ATF4: Activating transcription factor 4; MOI: Multiplicity of infection.

Competing interests

The authors declare that they have no competing interests.

Authors' contributions

HN, HL, KM, and HA performed the experimental studies, and KI helped to analyze the data. KM, MT, HA, YM, HO, NK, and AU participated in the characterization of iPSCs and their derivatives. HN, HL, and SF wrote the manuscript. NI revised the manuscript. All authors read and approved the final manuscript.

Acknowledgments

We especially thank M. Katata for excellent technical assistance. This work was partly supported by Grants-in-Aid for Scientific Research from the Ministry of Education, Culture, Sports, Science and Technology of Japan (24591616), the Ministry of Health, Labour and Welfare of Japan (H23-Jisedai-Ippan-001), and the Grants of National Center for Child Health and Development (22A-9 and 24–17).

Author details

[1]Department of Infectious Diseases, National Research Institute for Child Health and Development, 2-10-1 Okura, Setagaya-ku, Tokyo 157-8535, Japan. [2]Department of Reproductive Biology, Center for Regenerative Medicine, National Research Institute for Child Health and Development, 2-10-1 Okura, Setagaya-ku, Tokyo 157-8535, Japan. [3]Department of Pediatric Hematology and Oncology Research, National Research Institute for Child Health and Development, 2-10-1 Okura, Setagaya-ku, Tokyo 157-8535, Japan. [4]Department of Virology I, National Institute of Infectious Diseases, 1-23-1 Toyama, Shinjuku-ku, Tokyo 162-8640, Japan.

Received: 17 April 2013 Accepted: 15 October 2013
Published: 21 October 2013

References

1. Cheeran MC, Lokensgard JR, Schleiss MR: **Neuropathogenesis of congenital cytomegalovirus infection: disease mechanisms and prospects for intervention.** *Clin Microbiol Rev* 2009, **22**(1):99–126. Table of Contents.
2. Revello MG, Gerna G: **Diagnosis and management of human cytomegalovirus infection in the mother, fetus, and newborn infant.** *Clin Microbiol Rev* 2002, **15**(4):680–715.
3. Koyano S, Inoue N, Oka A, Moriuchi H, Asano K, Ito Y, Yamada H, Yoshikawa T, Suzutani T: **Screening for congenital cytomegalovirus infection using newborn urine samples collected on filter paper: feasibility and outcomes from a multicentre study.** *BMJ Open* 2011, **1**(1):e000118.
4. Cinatl J Jr, Vogel JU, Cinatl J, Weber B, Rabenau H, Novak M, Kornhuber B, Doerr HW: **Long-term productive human cytomegalovirus infection of a human neuroblastoma cell line.** *Int J Cancer* 1996, **65**(1):90–96.
5. Cinatl J Jr, Cinatl J, Vogel JU, Kotchetkov R, Driever PH, Kabickova H, Kornhuber B, Schwabe D, Doerr HW: **Persistent human cytomegalovirus infection induces drug resistance and alteration of programmed cell death in human neuroblastoma cells.** *Cancer Res* 1998, **58**(2):367–372.
6. Luo MH, Fortunato EA: **Long-term infection and shedding of human cytomegalovirus in T98G glioblastoma cells.** *J Virol* 2007, **81**(19):10424–10436.
7. Ogura T, Tanaka J, Kamiya S, Sato H, Ogura H, Hatano M: **Human cytomegalovirus persistent infection in a human central nervous system cell line: production of a variant virus with different growth characteristics.** *J Gen Virol* 1986, **67**(Pt 12):2605–2616.
8. Odeberg J, Wolmer N, Falci S, Westgren M, Seiger A, Soderberg-Naucler C: **Human cytomegalovirus inhibits neuronal differentiation and induces apoptosis in human neural precursor cells.** *J Virol* 2006, **80**(18):8929–8939.
9. Odeberg J, Wolmer N, Falci S, Westgren M, Sundtrom E, Seiger A, Soderberg-Naucler C: **Late human cytomegalovirus (HCMV) proteins inhibit differentiation of human neural precursor cells into astrocytes.** *J Neurosci Res* 2007, **85**(3):583–593.
10. Cheeran MC, Jiang Z, Hu S, Ni HT, Palmquist JM, Lokensgard JR: **Cytomegalovirus infection and interferon-gamma modulate major histocompatibility complex class I expression on neural stem cells.** *J Neurovirol* 2008, **14**(5):437–447.
11. Matsukage S, Kosugi I, Kawasaski H, Miura K, Kitani H, Tsutsui Y: **Mouse embryonic stem cells are not susceptible to cytomegalovirus but acquire susceptibility during differentiation.** *Birth Defects Res A Clin Mol Teratol* 2006, **76**(2):115–125.
12. Li RY, Tsutsui Y: **Growth retardation and microcephaly induced in mice by placental infection with murine cytomegalovirus.** *Teratology* 2000, **62**(2):79–85.
13. Kosugi I, Shinmura Y, Kawasaki H, Arai Y, Li RY, Baba S, Tsutsui Y: **Cytomegalovirus infection of the central nervous system stem cells from mouse embryo: a model for developmental brain disorders induced by cytomegalovirus.** *Lab Invest* 2000, **80**(9):1373–1383.
14. Nishino K, Toyoda M, Yamazaki-Inoue M, Fukawatase Y, Chikazawa E, Sakaguchi H, Akutsu H, Umezawa A: **DNA methylation dynamics in human induced pluripotent stem cells over time.** *PLoS Genet* 2011, **7**(5):e1002085.
15. Makino H, Toyoda M, Matsumoto K, Saito H, Nishino K, Fukawatase Y, Machida M, Akutsu H, Uyama T, Miyagawa Y, *et al*: **Mesenchymal to embryonic incomplete transition of human cells by chimeric OCT4/3 (POU5F1) with physiological co-activator EWS.** *Exp Cell Res* 2009, **315**(16):2727–2740.
16. Chambers SM, Fasano CA, Papapetrou EP, Tomishima M, Sadelain M, Studer L: **Highly efficient neural conversion of human ES and iPS cells by dual inhibition of SMAD signaling.** *Nat Biotechnol* 2009, **27**(3):275–280.

17. Nakamura H, Lu M, Gwack Y, Souvlis J, Zeichner SL, Jung JU: **Global changes in Kaposi's sarcoma-associated virus gene expression patterns following expression of a tetracycline-inducible Rta transactivator.** *J Virol* 2003, **77**(7):4205–4220.
18. White EA, Clark CL, Sanchez V, Spector DH: **Small internal deletions in the human cytomegalovirus IE2 gene result in nonviable recombinant viruses with differential defects in viral gene expression.** *J Virol* 2004, **78**(4):1817–1830.
19. Pevny LH, Sockanathan S, Placzek M, Lovell-Badge R: **A role for SOX1 in neural determination.** *Development* 1998, **125**(10):1967–1978.
20. Calfon M, Zeng H, Urano F, Till JH, Hubbard SR, Harding HP, Clark SG, Ron D: **IRE1 couples endoplasmic reticulum load to secretory capacity by processing the XBP-1 mRNA.** *Nature* 2002, **415**(6867):92–96.
21. Sidrauski C, Walter P: **The transmembrane kinase Ire1p is a site-specific endonuclease that initiates mRNA splicing in the unfolded protein response.** *Cell* 1997, **90**(6):1031–1039.
22. Scheuner D, Song B, McEwen E, Liu C, Laybutt R, Gillespie P, Saunders T, Bonner-Weir S, Kaufman RJ: **Translational control is required for the unfolded protein response and in vivo glucose homeostasis.** *Mol Cell* 2001, **7**(6):1165–1176.
23. Luo MH, Hannemann H, Kulkarni AS, Schwartz PH, O'Dowd JM, Fortunato EA: **Human cytomegalovirus infection causes premature and abnormal differentiation of human neural progenitor cells.** *J Virol* 2010, **84**(7):3528–3541.
24. Mutnal MB, Cheeran MC, Hu S, Lokensgard JR: **Murine cytomegalovirus infection of neural stem cells alters neurogenesis in the developing brain.** *PLoS One* 2011, **6**(1):e16211.
25. Grassi MP, Clerici F, Perin C, D'Arminio Monforte A, Vago L, Borella M, Boldorini R, Mangoni A: **Microglial nodular encephalitis and ventriculoencephalitis due to cytomegalovirus infection in patients with AIDS: two distinct clinical patterns.** *Clin Infect Dis* 1998, **27**(3):504–508.
26. Perlman JM, Argyle C: **Lethal cytomegalovirus infection in preterm infants: clinical, radiological, and neuropathological findings.** *Ann Neurol* 1992, **31**(1):64–68.
27. Isler JA, Skalet AH, Alwine JC: **Human cytomegalovirus infection activates and regulates the unfolded protein response.** *J Virol* 2005, **79**(11):6890–6899.
28. Skaletskaya A, Bartle LM, Chittenden T, McCormick AL, Mocarski ES, Goldmacher VS: **A cytomegalovirus-encoded inhibitor of apoptosis that suppresses caspase-8 activation.** *Proc Natl Acad Sci U S A* 2001, **98**(14):7829–7834.
29. Terhune S, Torigoi E, Moorman N, Silva M, Qian Z, Shenk T, Yu D: **Human cytomegalovirus UL38 protein blocks apoptosis.** *J Virol* 2007, **81**(7):3109–3123.
30. Schwartz RE, Trehan K, Andrus L, Sheahan TP, Ploss A, Duncan SA, Rice CM, Bhatia SN: **Modeling hepatitis C virus infection using human induced pluripotent stem cells.** *Proc Natl Acad Sci U S A* 2012, **109**(7):2544–2548.
31. Wu X, Robotham JM, Lee E, Dalton S, Kneteman NM, Gilbert DM, Tang H: **Productive hepatitis C virus infection of stem cell-derived hepatocytes reveals a critical transition to viral permissiveness during differentiation.** *PLoS Pathog* 2012, **8**(4):e1002617.
32. Lee KS, Zhou W, Scott-McKean JJ, Emmerling KL, Cai GY, Krah DL, Costa AC, Freed CR, Levin MJ: **Human sensory neurons derived from induced pluripotent stem cells support varicella-zoster virus infection.** *PLoS One* 2012, **7**(12):e53010.
33. D'Aiuto L, Di Maio R, Heath B, Raimondi G, Milosevic J, Watson AM, Bamne M, Parks WT, Yang L, Lin B, *et al*: **Human induced pluripotent stem cell-derived models to investigate human cytomegalovirus infection in neural cells.** *PLoS One* 2012, **7**(11):e49700.

doi:10.1186/2042-4280-4-2
Cite this article as: Nakamura *et al.*: Human cytomegalovirus induces apoptosis in neural stem/progenitor cells derived from induced pluripotent stem cells by generating mitochondrial dysfunction and endoplasmic reticulum stress. *Herpesviridae* 2013 **4**:2.

Submit your next manuscript to BioMed Central and take full advantage of:

- Convenient online submission
- Thorough peer review
- No space constraints or color figure charges
- Immediate publication on acceptance
- Inclusion in PubMed, CAS, Scopus and Google Scholar
- Research which is freely available for redistribution

Submit your manuscript at
www.biomedcentral.com/submit

BioMed Central

A synthetic nanofibrillar matrix promotes *in vitro* hepatic differentiation of embryonic stem cells and induced pluripotent stem cells

Taiji Yamazoe[1,2,3], Nobuaki Shiraki[1], Masashi Toyoda[4], Nobutaka Kiyokawa[4], Hajime Okita[4], Yoshitaka Miyagawa[4], Hidenori Akutsu[4], Akihiro Umezawa[4], Yutaka Sasaki[2], Kazuhiko Kume[1] and Shoen Kume[1,3,5,*]

[1]Division of Stem Cell Biology, Institute of Molecular Embryology and Genetics, Kumamoto University, Honjo 2-2-1, Kumamoto 860-0811, Japan
[2]Department of Gastroenterology and Hepatology, Faculty of Life Science, Kumamoto University, Honjo 2-2-1, Kumamoto 860-0811, Japan
[3]G.COE, Kumamoto University, Honjo 2-2-1, Kumamoto 860-0811, Japan
[4]Department of Reproductive Biology, National Institute for Child Health and Development, Okura 2-10-1, Setagaya, Tokyo 157-8535, Japan
[5]Program for Leading Graduate Schools "HIGO (Health life science; Interdisciplinary and Glocal Oriented) Program", Kumamoto University, Honjo 221, Chuoku, Kumamoto 8600811, Japan
*Author for correspondence (skume@kumamoto-u.ac.jp)

Accepted 9 September 2013
Journal of Cell Science 126, 5391–5399
© 2013. Published by The Company of Biologists Ltd
doi: 10.1242/jcs.129767

Summary

Embryonic stem (ES) cells recapitulate normal developmental processes and serve as an attractive source for routine access to a large number of cells for research and therapies. We previously reported that ES cells cultured on M15 cells, or a synthesized basement membrane (sBM) substratum, efficiently differentiated into an endodermal fate and subsequently adopted fates of various digestive organs, such as the pancreas and liver. Here, we established a novel hepatic differentiation procedure using the synthetic nanofiber (sNF) as a cell culture scaffold. We first compared endoderm induction and hepatic differentiation between murine ES cells grown on sNF and several other substrata. The functional assays for hepatocytes reveal that the ES cells grown on sNF were directed into hepatic differentiation. To clarify the mechanisms for the promotion of ES cell differentiation in the sNF system, we focused on the function of Rac1, which is a Rho family member protein known to regulate the actin cytoskeleton. We observed the activation of Rac1 in undifferentiated and differentiated ES cells cultured on sNF plates, but not in those cultured on normal plastic plates. We also show that inhibition of Rac1 blocked the potentiating effects of sNF on endoderm and hepatic differentiation throughout the whole differentiation stages. Taken together, our results suggest that morphological changes result in cellular differentiation controlled by Rac1 activation, and that motility is not only the consequence, but is also able to trigger differentiation. In conclusion, we believe that sNF is a promising material that might contribute to tissue engineering and drug delivery.

Key words: Hepatic differentiation, *In vitro* differentiation, Embryonic stem cells, Induced pluripotent stem cells

Introduction

The liver is an important organ that performs many complex functions, including the metabolism of carbohydrates, proteins and lipids, as well as storage of essential nutrients and biotransformation of drugs. Drug biotransformation involves detoxification and bioactivation, where the metabolite becomes more toxic. Therefore, drug biotransformation plays an important role in the early stages of drug discovery processes. Primary hepatocyte cultures are often used for pharmacological assays, but they are short-lived and cannot be maintained in long-term culture. In addition, there are considerable donor-dependent variations. By contrast, embryonic stem (ES) cells or induced pluripotent stem (iPS) cells can proliferate infinitely and maintain their pluripotent ability to differentiate into various cell types. There is evidence that ES or iPS cells recapitulate normal developmental processes, and can serve as an alternative resource for hepatological researches, drug development and clinical uses. Through our present knowledge of developmental biology, efficient induction of hepatic lineage cells has been established. For example, based on the evidence that TGFβ–activin–Smad2 signaling is involved in definitive endoderm formation in the mouse (Tremblay et al., 2000), the activation of Activin–Nodal signaling was used for endoderm induction (D'Amour et al., 2005; Kubo et al., 2004). Fibroblast growth factor (FGF) and bone morphogenetic protein (BMP) were added for the specification of liver lineages (Jung, 1999; Mfopou et al., 2010; Shiraki et al., 2008a); this helped to mimic the mesodermal signals from the septum transversum mesenchyme in normal development (Katsumoto et al., 2010; Shin et al., 2007; Rossi et al., 2001). Because hepatocyte growth factors are known to be important effectors in the specification of cell fate and organogenesis of the liver (Schmidt et al., 1995; Sonnenberg et al., 1993), hepatocyte growth factor (HGF), dexamethasone and oncostatin M have been used for induction of hepatocyte maturation (Basma et al., 2009; Kamiya et al., 1999; Si-Tayeb et al., 2010). Compared with the factors described above that direct hepatic differentiation, the role of extracellular matrices (ECMs) and scaffolds remains unclear.

Journal of Cell Science

Journal of Cell Science

We have previously reported that culturing ES/iPS cells on the mesonephric M15 cell line, in the presence of specific growth factors, resulted in an efficient induction of endoderm-derived tissues, such as the liver or pancreas (Shiraki et al., 2008a; Shiraki et al., 2008b; Umeda et al., 2013). We further suggested that the basement membrane components, including *lama5*, play an important role in guiding the differentiation of ES cells into regional-specific lineages of the definitive endoderm (Higuchi et al., 2010). We also successfully established an alternative hepatic differentiation procedure without using feeder cells, but with a synthesized basement membrane (sBM) substratum (Higuchi et al., 2010; Shiraki et al., 2011). Together, these results revealed the importance of the ECM for differentiation of ES cells.

The basement membrane, a highly integrated three-dimensional structure composed of ECM molecules, is known to regulate various cellular processes. It is known that electrospun nanofibers provide not only three-dimensional microenvironments mimicking the ECM, but also appropriate guidance cues to modulate cell behavior. Here, we tested the effects of synthetic nanofiber (sNF) matrices on ES/iPS cell differentiation. We found that ES/iPS cells grown on the sNF were induced into endoderm and then hepatic fates. Overall, we conclude that the sNF is more potent in promoting hepatic differentiation, compared with the traditional two-dimensional culture surfaces, and is able to substitute for the sBM or M15 cells.

Results

Differentiation of murine and human ES cells into the hepatic lineages on the sNF matrix

We first tested the sNF matrix for its potency to mimic the basement membrane substratum of the cells. Murine SK7 ES cells (Shiraki et al., 2008a) were seeded onto the sNF matrix, and allowed to differentiate into the hepatic lineage by sequential changes of medium containing specific growth factors (Fig. 1A). We found that the expression of the pluripotent marker *Oct3/4* was downregulated, whereas the mesendoderm marker *Gsc* and definitive endoderm markers *Sox17* and *Foxa2* were expressed at day 4 (d4) of differentiation (Fig. 1B). Whereas *Gsc* was downregulated rapidly, *Sox17* and *Foxa2* showed peak expressions around d7 and were downregulated afterwards. Notably, the hepatic progenitor marker gene, alpha-fetoprotein (*Afp*), and the mature hepatocyte marker, albumin (*Alb1*) were detectable from d12 and d16, respectively, and their expression levels were increased with time. Although the *Afp* transcript level was decreased after d22, the *Alb1* expression continued increasing beyond d22. The immunocytochemical analysis further confirms that ALB and AFP were present in the cytoplasm of differentiated ES cells (Fig. 1C). In addition, periodic-acid–Schiff (PAS) staining and the Indocyanin Green (ICG) test were also conducted to investigate the hepatocyte functions of differentiated ES cells. The former reflects glycogen storage by showing positive populations as magenta in the cytoplasm, and the latter is used to examine cellular uptake activities, which are regarded as a hepatocyte detoxification function. As shown in Fig. 1D, glycogen storage was observed as the accumulation of magenta staining in the cytoplasm of the differentiated cells (top panel) and the ICG test also shows a similar result (bottom panel).

We next investigated whether human ES or iPS cells could differentiate in the sNF system. We used khES3 human ES cells

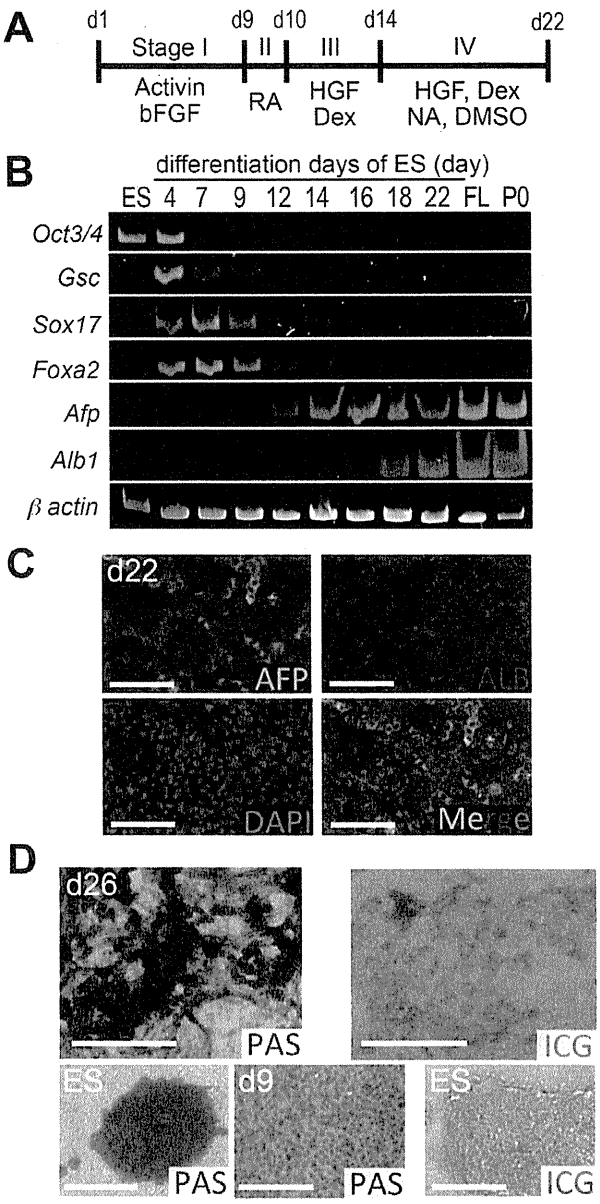

Fig. 1. Differentiation of murine ES cells into the hepatocyte lineage on nanofiber scaffolds. (A) Schematic diagram of the differentiation procedure for mouse ES cells. (B) Time-dependent expression levels of endoderm and hepatic marker genes. β-actin was used as a control. FL, fetal liver on embryonic day 12.5; P0, neonatal liver on postnatal day 0. (C) The immunochemical analysis of differentiated ES cells on day 22 (d22) for α-fetoprotein (AFP, green) and albumin (ALB, red) with nuclear counterstaining (DAPI). (D) Hepatocyte functional tests for PAS and ICG on d26 differentiated ES cells (top panels) and undifferentiated (bottom left and right panels) and d9 differentiated (bottom middle panel) ES cells as negative controls (bottom panels). Nuclei are counterstained with hematoxylin (blue). Scale bars: 250 μm.

(supplementary material Fig. S1A–D), as well as human iPS cell lines, such as Toe (supplementary material Fig. S1E,G) and 201B7 (supplementary material Fig. S1F), and found that these cells were able to differentiate into hepatocyte-like cells, thereby

producing ALB and taking up ICG (supplementary material Fig. S1D–G). Together, these results indicate that sNF is a suitable matrix for potentiating hepatic differentiation, not only in murine cells, but also in human ES cells and iPS cells.

sNF is more potent than normal plates precoated with other matrices

To compare the supportive effects of NFs and other substrata, we seeded murine ES cells onto either the sNF matrix or normal plates precoated with other stubstrata, including collagen I, Matrigel, gelatin and fibronectin and then performed the differentiation experiment as described in Fig. 1A. On differentiation day 22 (d22), quantitative PCR analyses were carried out to quantify the expression profiles of hepatic function marker genes in differentiated cells. Our results indicate that ES cells grown on sNF showed higher expression levels of proteins secreted by hepatocytes, such as serine peptidase inhibitor a1 (*Serpina1*), *Ttr* and *Alb1*, compared with those grown on other substrata (Fig. 2). Similar results were observed for the expression of several other genes, including glucose 6-phosphatase (*G6p*) and fatty-acid

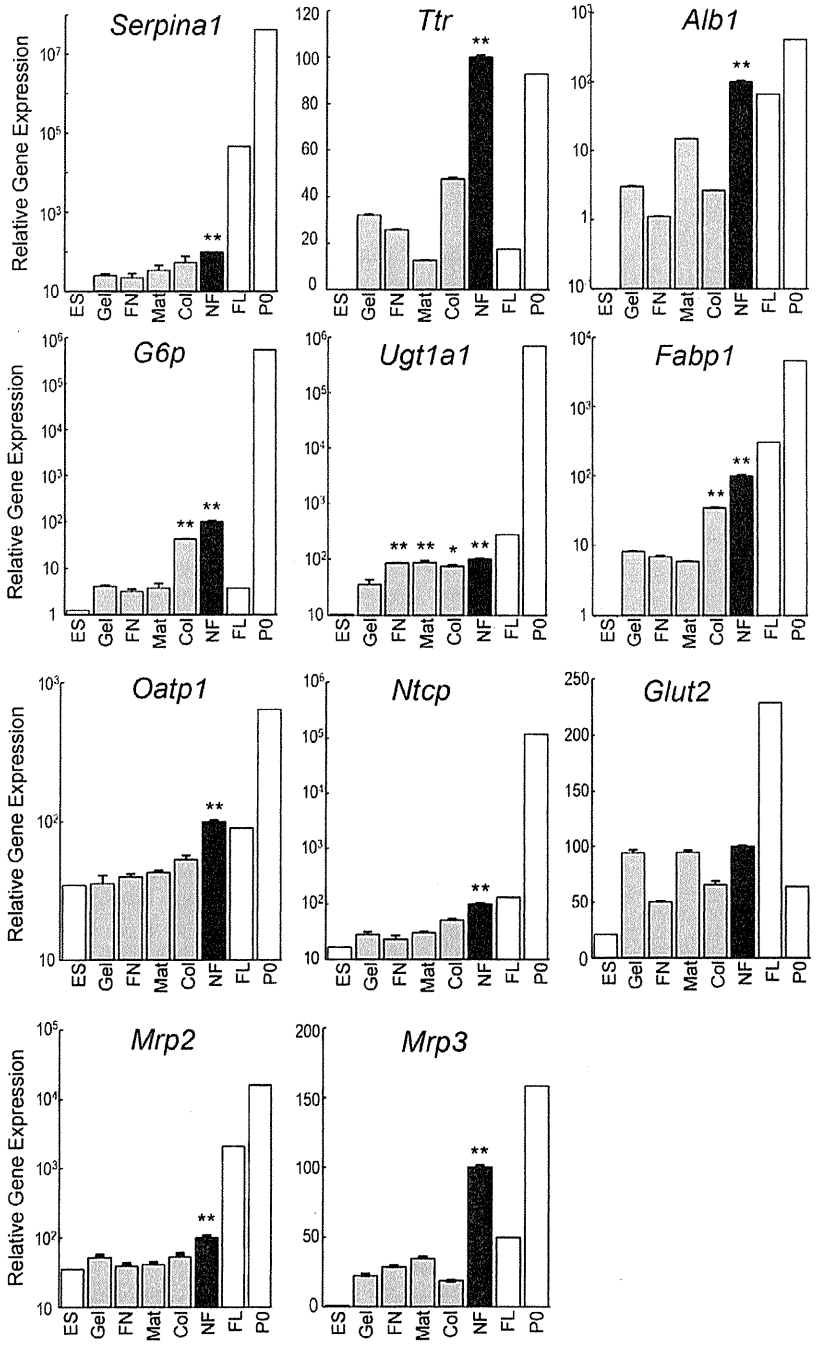

Fig. 2. Expression of hepatic markers in differentiated murine ES cells on sNF or other substrata. Expression levels of various gene transcripts quantified by real time PCR in d22 differentiated ES cells cultured on sNF, collagen I (Col), Matrigel (Mat), fibronectin (FN) or gelatin (Gel). ES, undifferentiated ES cells. FL (E12.5 fetal liver) and P0 (neonatal liver on postnatal day 0) are used as references. For differentiated ES cells, values represent mean ± s.e.m. (n=3). *P<0.05 and **P<0.01, by one-way ANOVA with the post-hoc Dunnett's test.

Journal of Cell Science

binding protein (*Fabp1*), or transporters, such as organic anion-transporting polypeptide 1 (*Oatp1*), Na^+-taurocholate cotransporting polypeptide (*Ntcp*) and UDP-glucuronosyltransferase (*Ugt1a1*), as well as multidrug resistance-associated protein family proteins 2 and 3 (*Mrp2* and *Mrp3*) (Fig. 2). By contrast, little change was found in the expression of glucose transporter 2 (*Glut2*).

To determine the hepatic functions of differentiated ES cells grown on Matrigel, collagen I or sNF, we next measured their ALB secretions, ICG uptake and cytochrome p450 (CYP) activities. Our results show that ES cells grown on sNF secreted ALB at a higher level compared with those on Matrigel or collagen I (Fig. 3A). By day 26, the percentage of ICG-positive ES cells on sNF was also higher than in ES cells grown on the other two substrates (Fig. 3B,C).

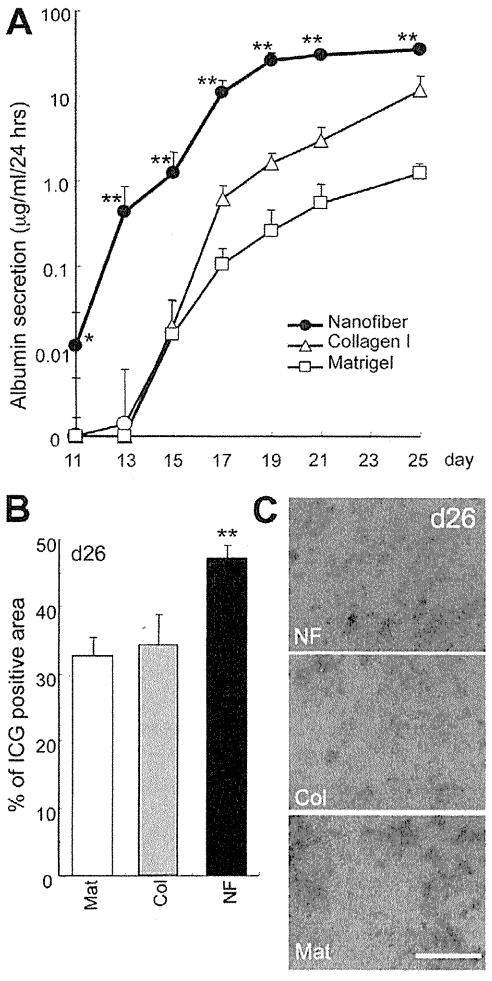

Fig. 3. Liver functional assays of differentiated murine ES cells grown on nanofiber scaffolds versus other substrata. (A) ELISA analysis of time-dependent albumin secretion for 24 hours by ES cells grown on Matrigel (Mat), collagen I (Col) or NF. (B,C) ICG tests performed on d26 differentiatied ES cells. The percentage of cells taking up ICG in culture was calculated (B) and representative images are shown (C). Values represent means ± s.e.m. (n=6). *P<0.05, **P<0.01, by two-tailed Student's t-test. Scale bar: 250 μm.

To measure CYP activities, the differentiated ES cells were treated with a CYP1A inducer, 3-methylcholantrene (3MC), for 48 hours during d22–d24 or d64–d66, as shown in supplementary material Fig. S2A. We found that the differentiated cells cultured on sNF had higher CYP1A1 activities and responses to the inducer than those cultured on fibronectin, Matrigel or collagen I (supplementary material Fig. S2B). We also assayed the effects of sNF on the maintenance of the mature hepatic cells. ES cells cultured on sNF were able to maintain their CYP1A1 activities and responses to 3MC even on d66, whereas those cultured on other matrices did not survive in long-term cultures (supplementary material Fig. S2C). It is also worth noting that the differentiated cells on sNF could be maintained in culture for more than 100 days. Specifically, we show that the ES cells cultured on sNF for 129 days were able to uptake and secrete ICG (supplementary material Fig. S2D). Based on these findings, we conclude that sNF is an excellent matrix, not only for the differentiation of ES cells into the hepatic lineage but also for maintaining the mature state of ES-cell-derived hepatocytes.

High Rac1 activities in undifferentiated and differentiated ES cells grown on sNF

Next, we investigated the effects of sNF on hepatic differentiation of ES cells. It was previously reported that the undifferentiated murine ES cells cultured on sNF exhibited spheroid morphologies and formed dome-like structures, and proliferated well (Nur-E-Kamal et al., 2006). Therefore, we checked the morphological changes between the undifferentiated and differentiated states of the murine ES cells. To exclude the effect of the extracellular matrix, we compared gelatin-coated normal two-dimensional (2D) plates with either gelatin-coated or uncoated sNF. We found that the undifferentiated ES cells grown on gelatin-coated 2D plates, with cytoplasmic spreading morphologies and attached to the plate surface in large areas (Fig. 4A, left). By contrast, the ES cells grown on sNF showed aggregated morphologies (Fig. 4A, middle and right).

In the differentiated state, the ES cells were found to form a monolayer on sNF. However, the morphological differences were still observed between ES cells cultured on sNF or normal 2D plates (Fig. 4B). Because these morphological changes are known to be regulated by cytoskeletal molecules, such as small Rho GTPase family member proteins, we next examined Rac1 activities in undifferentiated and differentiated ES cells. Our western blot analyses demonstrate that the GTP-bound active form of Rac1 was expressed at a higher level in ES cells cultured on sNF than those cultured on normal 2D plates, even though total Rac1 expression levels were similar (Fig. 4C,D). Interestingly, both the undifferentiated (Fig. 4C) and the differentiated ES cells on d8 (Fig. 4D) showed higher Rac-GTP activities. These results not only agree with the morphological differences of the ES cells, but also suggest that activated Rac1 plays a crucial role in potentiating the differentiation activity of ES cells cultured on sNF into hepatic lineages.

A crucial role of Rac activation in potentiating the differentiation of ES cells into the definitive endoderm and hepatocyte lineages

NSC23766 is a selective inhibitor of Rac1 activation that is mediated by the Rac-specific guanine nucleotide exchange factors (GEFs) TrioN and Tiam1, without affecting other Rho

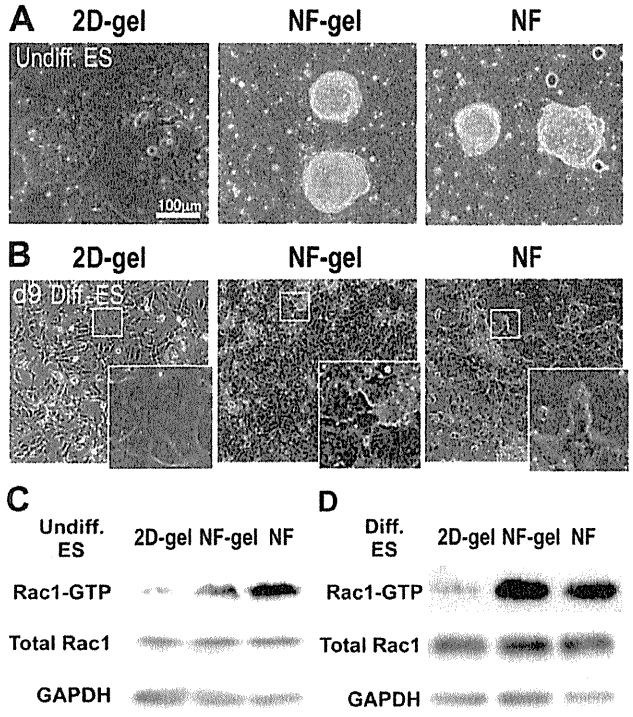

Fig. 4. NF induces Rac1 hydroxylation in both undifferentiated and day 9 differentiated murine ES cells. (A,B) Representative images of undifferentiated (A) and day 9 (d9) differentiated (B) ES cells grown on gelatin-precoated normal plates (2D-gel), gelatin-coated NF plates (NF-gel) and uncoated NF plates (NF). Insets are higher magnifications of the boxed regions. (C,D) Western blot analysis of GTP-bound active Rac1, total Rac1 and GAPDH expression in undifferentiated (C) or differentiated (D) ES cells described in A,B.

family members, such as RhoA or Cdc42 (Gao et al., 2004). We confirmed that 100 μM NSC23766 inhibited Rac1 hydroxylation (supplementary material Fig. 3A). To test whether sNF potentiates the differentiation of ES cells into the hepatic lineages through Rac1 activation, we treated murine ES cells with 100 μM NSC23766 at various stages and then determined the expression of stage-specific markers (Fig. 5A–C). We first added NSC23766 for 4 days at stage I to examine the effect of Rac1 activation on endoderm induction (Fig. 5A). We found that *Foxa2* expression was downregulated by the Rac1 inhibitor in ES cells cultured on sNF (Fig. 5A). We next examined the effects of Rac1 inhibition on hepatic differentiation. Our results show that the Rac1 inhibitor added at stage II (Fig. 5B) or stage III (Fig. 5C) downregulated the expression of hepatic markers, *Afp* or *Alb1*, on d10 or d14, respectively.

These results suggested that Rac1 activation is crucial for endoderm and hepatic differentiation. We subsequently examined the stage dependency of hepatic differentiation on Rac1 activities. The Rac1 inhibitor was added at different stages (I, II, III or IV) and *Alb1* expression was assayed on day 18 (Fig. 5D). We found that Rac1 inhibition at all four stages blocked the potentiating effects of sNF, and resulted in decreases in *Alb1* expression. These results further confirm the important role of Rac1 and demonstrate that continuous activation of Rac1 is crucial for the potentiation of hepatic differentiation.

Then we confirmed whether NSC23766 had any effect on the proliferation of ES cells. NSC23766 decreased the proportion of EdU-positive cells in stages I, II and III, particularly in stage I, without apparent toxicity (supplementary material Fig. S3C). Interestingly, the total numbers of cells in the NSC23766-treated groups was smaller in stages I and II, which became greater than that of control groups used in stages III and IV (supplementary material Fig. S3B). Taken together, these findings suggest that Rac1 differentially contributes to proliferation in the early differentiation stages and promotes differentiation in the late stage.

Discussion

Our previous study suggested that although addition of soluble growth factors is sufficient to promote the differentiation of ES cells into the definitive endoderm, further differentiation from the definitive endoderm into hepatic and pancreatic fates appears to require a direct contact with M15 cells (Shiraki et al., 2008a). We previously showed the importance of basement membrane substratum by culturing ES cells on sBM (Higuchi et al., 2010; Shiraki et al., 2011). Specifically, ES cells grown on sBM were able to differentiate into hepatic and pancreatic lineages. These results imply that the basement membrane structure plays a major role in the differentiation of ES cells. Although the sBM used previously was constructed by overexpressing recombinant laminin-511 (laminin α5, laminin β1 and laminin γ1) in H293 cells (Doi et al., 2002), ES cells or iPS cells could be induced into the hepatic and pancreatic lineages. The efficacy of such an sBM for differentiation was high, and the differentiated cells could perform liver-specific functions, such as protein secretion, detoxification and glycogen storage (Higuchi et al., 2010; Shiraki et al., 2011).

The nanofiber produced by the electrospinning technique is a chemically and physically stable synthetic three-dimensional surface that mimics the structural geometry and porosity of the basement membrane or ECM (Schindler et al., 2005; Schindler et al., 2006). NF scaffolds have been shown to recapitulate the structural features of stem cell niche (Lim and Mao, 2009) and have been used for the *ex vivo* expansion of various types of stem cells such as murine ES cells (Hashemi et al., 2011; Nur-E-Kamal et al., 2006) and human tissue stem cells. In addition, the ECM was found to deposit as an extensive scaffold on the basal surface of the cells attached to NFs (Shih et al., 2006; Chua et al., 2007; Ma et al., 2008). Importantly, the sNF system has been reported to enhance not only the differentiation of murine ES cells into neural lineages (Lim et al., 2010; Purcell et al., 2012; Xie et al., 2009), but also differentiation from human MSCs into hepatoblasts (Ghaedi et al., 2012; Kazemnejad et al., 2009).

Taken together, these previous observations revealed that the sNF matrix is useful as a substratum to replace feeder cells and that it has the ability to potentiate hepatic differentiation. In this study, we show that both murine and human ES cells, as well as human iPS cells, could differentiate on sNF and exhibit liver-specific functions. Furthermore, we demonstrate that Rac1 activation was involved in hepatic differentiation. Rac1, a member of the Rho family GTP-binding proteins, including Rho and Cdc42 (Heasman and Ridley, 2008), functions by activating actin-rich lamellipodial protrusion and membrane ruffling, which are thought to be a major part of the driving force for cell movement (Nobes and Hall, 1995; Ridley et al., 1992). Although Rho family proteins were reported to be

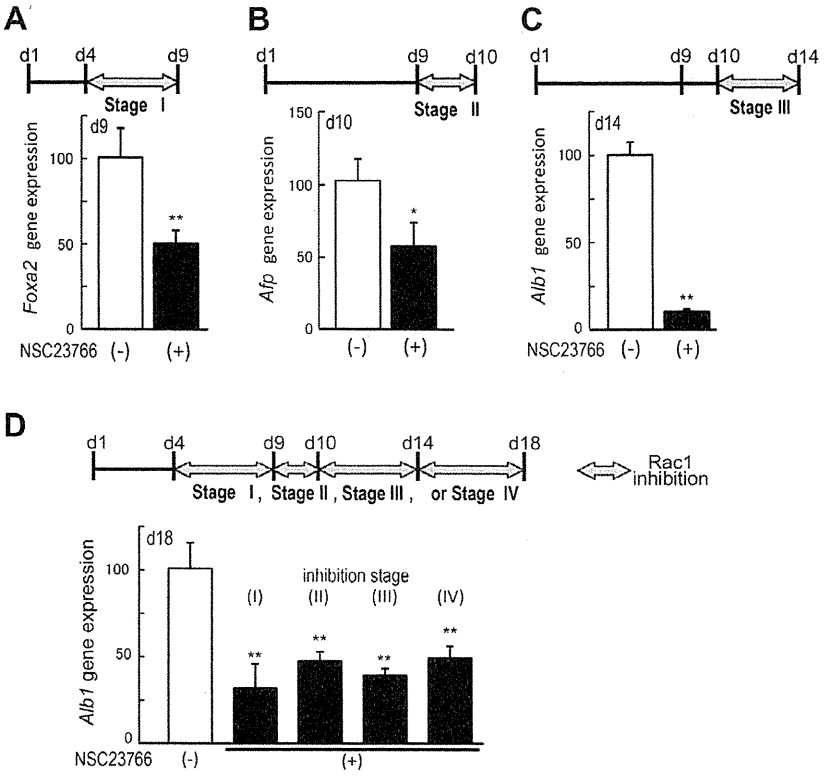

Fig. 5. Inhibition of the Rac1 pathway blocks the differentiation-potentiating activity of NF. (A–C) Quantitative PCR analysis of the gene expression of *Foxa2* (A), *Afp* (B) and *Alb1* (C), in differentiated cells cultured on sNF with (+) or without (−) the Rac1 inhibitor NSC23766 (100 μM), at the end of stage I (A), stage II (B) or stage III (C). (D) The expression of *Alb1* on day 18 in differentiated cells, treated with (+) or without (−) the Rac1 inhibitor at indicated stages. Data shown represent mean ± s.e.m. (n=3); *P<0.05 and **P<0.01, compared with untreated cells on sNF with the Rac1 inhibitor by two-tailed Student's t-test or one-way ANOVA with the post-hoc Dunnett's test.

expressed by ES cells cultured on sNF (Nur-E-Kamal et al., 2005; Nur-E-Kamal et al., 2006; Schindler et al., 2006), their roles have never been investigated.

In vivo developmental processes occurring in the endoderm and its derivatives cause dynamic migration during gastrulation and later stages of organogenesis (Woo et al., 2012), suggesting that motility and differentiation are closely inter-related. In this study, we observed that ES cells cultured on sNF showed greater Rac1 activation than did cells cultured on the normal 2D surface. Indeed, Rac1 is known to be involved in not only endoderm induction but also hepatic specification and maturation. In particular, *Rac1* mutant mice died by mouse embryonic day 9.5 (E9.5) because of severe developmental abnormalities, and *Rac1*-deficient embryos showed numerous cell deaths in the space between the ectoderm and endoderm at the primitive streak stage (Sugihara et al., 1998). Rac1 is also important for cellular differentiation, for example, epithelial differentiation in the small intestine (Stappenbeck and Gordon, 2000), pancreatic islet morphogenesis (Greiner et al., 2009), myogenic differentiation (Heller et al., 2001), maintenance of the thymic epithelial cells (Hunziker et al., 2011), formation of the lens (Maddala et al., 2011) and neuronal development (Corbetta et al., 2009; Leone et al., 2010). In addition, Rac1 has been shown to crosstalk with many downstream signaling pathways such as Wnt (Clarke, 2006; Malliri et al., 2006), TGF-β1 (Varon et al., 2008), Nodal (Woo et al., 2012), retinoic acid (Lee et al., 2008) and Myc (Hunziker et al., 2011; Nikolova et al., 2008). Interestingly, Rac1 is also known to mediate stem cell-shape-dependent regulation of differentiation to a chondrogenic versus myogenic fate (Gao et al., 2010). On the basis of these studies, we postulate that the sNF system might potentiate ES cells to differentiate into hepatic lineages by interacting downstream of certain growth factors during differentiation processes.

In conclusion, we show that Rac1 was activated in both undifferentiated and differentiated ES cells cultured on sNF plates and that Rac1 inhibition blocked the potentiating effects of sNF on endoderm and hepatic differentiation. These results suggest that continuous activation of Rac1 throughout the differentiation stage is crucial for potentiating differentiation. Our results also highlight the morphological changes during differentiation along the Rac1 pathway, which controls cellular morphology, motility and differentiation into the hepatic lineage. Here, we established a completely chemically defined method that requires no serum or no xenogenic substrata, thereby eliminating the risk of contamination with unknown factors. We believe that this novel method could be an attractive culture model for pharmacological research and research on stem cell biology and therapeutic strategies.

Materials and Methods

ES and iPS cell lines

The murine ES cell line, SK7 (Shiraki et al., 2008a) was maintained on mouse embryonic fibroblast (MEF) feeders in Glasgow minimum essential medium (Invitrogen, Glasgow, UK) supplemented with 1000 units/ml leukemia inhibitory factor (LIF; Chemicon, Temecula, CA), 15% knocked-out serum replacement (KSR; Invitrogen), 1% fetal bovine serum (FBS; Hyclone, Logan, UT), 100 μM nonessential amino acids (NEAA; Invitrogen), 2 mM L-glutamine (L-Gln; Invitrogen), 1 mM sodium pyruvate (Invitrogen), 50 units/ml penicillin and 50 μg/ml streptomycin (PS; Invitrogen) and 100 μM β-mercaptoethanol (β-ME; Sigma-Aldrich, St Louis, MO).

Human ES cells (KhES-3) (Suemori et al., 2006) were from Dr Norio Nakatsuji and Dr Hirofumi Suemori (Kyoto University, Kyoto, Japan). They were used in accordance with the human ES cell guidelines of the Japanese government. This human ES work was approved by Kumamoto University institutional review board. Human iPS 201B7 cells were a gift from Dr Yamanaka (Kyoto University, Kyoto, Japan). The human iPS Toe cell line was established by M. Toyoda and

Journal of Cell Science

colleagues (National Institute for Child Health and Development, Tokyo, Japan). Undifferentiated human ES and iPS cells were maintained as described previously (Shiraki et al., 2008b).

Culture plates

Synthetic nanofiber (sNF) matrices were purchased from Corning Coster (Ultra-Web Synthetic Polyamine Surface #3873XX1; Cambridge, MA). Plate surfaces were coated with electrospun polyamide nanofibers. sNF matrices consisted of two kinds of polyamide polymers, A $(C_{28}O_4N_4H_{47})_n$ and B $(C_{28}O_{4.4}N_4H_{47})_n$, which were crosslinked in the presence of an acid catalyst, and were 200–400 nm in diameter (average 280 nm). Pore sizes, similar to those of the cell basement membrane, were ~700 nm. For comparison, Corning 96-well plates were pretreated for 3 hours at 37℃ with 0.1% gelatin (Sigma-Aldrich), Matrigel (BD, Franklin Lakes, NJ) or CellStart (Invitrogen). Collagen I (Nitta Gelatin, Japan) was diluted with Dulbecco's modified Eagle's medium (DMEM; Invitrogen) at a concentration of 1 mg/ml and plate surfaces were treated for 15 minutes, then dried until use.

Differentiation of murine ES cells into hepatic lineages on sNF

Murine ES cells plated at a density of 1.5×10^4 cells/cm^2 in culture plates described above were grown for 8 days in DMEM containing 4,500 mg/l glucose, s NEAA, L-Gln, PS, β-ME, 10 mg/ml insulin, 5.5 mg/ml transferrin, 6.7 pg/ml selenium (Insulin-Transferrin-Selenium-G Supplement; ITS, Invitrogen), 0.25% AlbuMAX II (Invitrogen), 10 ng/ml recombinant human activin-A (R&D Systems, Minneapolis, MN), 5 ng/ml; recombinant human bFGF, and cultured for 8 days. On day 9 (d9), the medium was changed to RPMI-1640 (Invitrogen) containing 10^{-6} M retinoic acid (RA; Stemolecule all-trans retinoic acid; Stemgent, Cambridge, MA) and B27 supplement (Invitrogen). On d10, medium was switched to 2000 mg/l glucose DMEM (Invitrogen), 10% KSR, 10 ng/ml recombinant human hepatocyte growth factor (Peprotech, Rocky Hill, NJ) and 10 μM dexamethasone (Sigma-Aldrich), and cultured until d14. Next, 1 mM nicotinamide (NA; Sigma-Aldrich) and 1% dimethylsufoxide (DMSO; Sigma-Aldrich), were added to medium and KSR was removed. Medium was replaced every 2 days with fresh medium and growth factors.

Human ES/iPS cells were pretreated with the ROCK inhibitor Y27632 (Wako, Japan) 1 day before trypsinization. Cells were plated at a density of 3×10^5 cells/cm^2 on Matrigel-coated sNF matrices with Y27632. The following two procedures were subsequently used to induce hepatic differentiation of various human ES/iPS cells; simplified (two-step) protocol, KhES3 and 201B7 cells; or conventional (three-step) protocol, Toe cells. In the simplified protocol, medium used at first contained B27 and 100 ng/ml activin-A in RPMI-1640, which was then, switched to 10 ng/ml HGF, 10 μM dexamethasone, 0.5% DMSO, 0.5 mM NA. In the conventional protocol, medium used first was the same as that in the simplified protocol, followed by 1% DMSO and 20% KSR in knockout DMEM/F12 (Invitrogen) for 6 days and, then DMEM containing HGF, dexamethasone and 10% KSR. Finally, the above medium was added with 0.5 mM NA. Medium was replaced every 2 days with fresh medium and growth factors. KhES3 and 201B7 cells were induced hepatic differentiation with simplified protocol, and Toe cells were treated with conventional protocol.

Periodic-acid–Schiff's staining

For detection of glycogen storage in the differentiated cells, periodic-acid–Schiff's (PAS) staining kit (Muto Pure Chemicals, Tokyo, Japan) was used. Cells cultured for 9 and 26 days, and undifferentiated ES cells were fixed in 3.3% formalin for 10 minutes, and stained following the manufacturer's instructions, then nuclear counterstaining with hematoxylin (blue) was performed.

Albumin secretion assay

The culture medium was replaced with fresh medium every 2 days, and supernatants were collected 24 hours after replacing the medium. The mouse (human) albumin secreted in the supernatant was determined using a mouse (human) ELISA quantification kit (Bethyl, Montgomery, TX).

Indocyanine Green (ICG) test

Indocyanine Green (Daiichi-Sankyo Pharm., Japan) was diluted with the above culture medium to a final concentration of 1 mg/dl. The ICG test solution was added to the differentiated ES cells after the appropriate culture periods and undifferentiated ES cells were used as controls, and incubated at 37℃ for 30 minutes. Then, after three washes with phosphate-buffered saline (PBS), the cellular uptake of ICG was examined by microscopy. The percentage ICG-positive areas represent the proportion of ICG-positive area versus total cell area, which were determined using ImageJ software (US National Institutes of Health, Bethesda, MD).

CYP inductions

To check the inducibilities of cytochrome P450 activities in response to inducers, we used the P450-Glo CYP Assay Kit (Promega, Madison, WI). The differentiated ES cells were treated with 5 μM 3-methylcholantrene as inducers of CYP1A. The medium containing the inducers was changed every 24 hours. 48 hours after treatment, we changed the medium and used the appropriate luminogenic CYP substrates (Luciferine-CEE for CYP1A). The cells were incubated at 37℃ for 3 hours, and then the supernatants were mixed with equal amount of detection reagent, according to the manufacturer's instructions. The luminescence was measured using a GloMax 96 microplate luminometer (Promega), and luminometer settings were as in the manufacturer's instructions. Cell numbers were calculated using CellTiter-Glo luminescent cell viability assays (Promega) to normalize P450-Glo assay values to cell number.

Immunocytochemistry

After culture for the appropriate times, cells were fixed in 4% paraformaldehyde in PBS for 30 minutes at room temperature. After removal of paraformaldehyde solution, the fixed cells were permeabilized with 0.1% Triton X-100 for 10 minutes. The permeabilized cells were rinsed several times with PBS and were then incubated with 20% Blocking One (Nacalai Tesque, Japan) in PBST (0.1% Tween-20 in PBS) for blocking. After blocking, the cells were incubated with the diluted antibody in 20% Blocking One in PBST (0.1% Tween-20 in PBS) in a humidified chamber overnight at 4℃. After washing the cells in PBST, cells were incubated with the secondary antibody in 20% Blocking One for 2 hours at room temperature in the dark. After washing off the secondary antibody in PBST, cells were counterstained with 6-diamidino-2-phenylindole (DAPI) (Roche Diagnostics, Switzerland). The following antibodies were used as primary antibodies: rabbit anti-alphafeto protein (Dako, Denmark), goat anti-albumin (Sigma-Aldrich), goat anti-Sox17, mouse anti-FoxA2 (R&D systems); secondary antibodies used were conjugated to Alexa Fluor 568, Alexa Fluor 488 and Alexa Fluor 633 (Invitrogen). For human ES cell cultures, goat antibodies against human albumin (Bethyl) were used as primary antibodies.

Cell proliferation assay

Cell proliferation was evaluated using Click-iT EdU assay kit (invitrogen). The cells cultured with or without NSC23766 were exposed to 10 μM of 5-ethnyl-2′-deoxyuridine (EdU) for 1 hour at 37℃ before fixation. The fixed cells were processed for immunocytochemistry as described above, with an additional step for EdU detection. Before incubation with secondary antibodies, the cells were incubated with EdU in the Click-iT reaction cocktail and Alexa Fluor 488 for 30 minutes at room temperature, following the manufacturer's instructions. Images were collected using ImageXpress Micro (Molecular Devices) and EdU-positive nuclei per total number of nuclei were counted.

RT-PCR analysis

RNA was extracted from ES cells or mouse liver using an RNeasy mini-kit (Qiagen, Germany) and then treated with DNase (Qiagen). For reverse transcription reactions, 3 μg RNA was reverse-transcribed using ReverTra Ace (Toyobo, Japan) and oligo dT primers (Toyobo). One μl of fivefold-diluted cDNA (1% of the RT product) was used for PCR analyses. The primer sequences for each primer set are shown in supplementary material Table S1. For real-time PCR analysis, mRNA expression was quantified with SyberGreen on an ABI 7500 thermal cycler (Applied Biosystems, Foster City, CA). The PCR conditions were as follows: denaturation at 95℃ for 15 seconds, annealing and extention at 60℃ for 60 seconds, for up to 40 cycles. Each measurement was normalized to β-actin (mouse) and *GAPDH* (human) for each sample by subtracting the average β-actin (mouse) and *GAPDH* (human) C_t values (Threshold Cycle) from the average C_t for each gene. Target mRNA levels, expressed as arbitrary units, were determined using a standard curve method.

Rac pull-down assay

Murine ES cells were trypsinized and suspended at a density of 5×10^4 cells/ml. Cells were then plated onto sNF either with or without 0.1% gelatin pretreatment; control plates were pretreated with 0.1% gelatin. Undifferentiated cells were harvested 48 hours after incubation under ES cell maintenance culture conditions at 37℃, whereas differentiated cells were harvested 9 days after hepatic differentiation started. The activation of Rac was determined using a Rac1 Activation Assay Kit purchased from Millipore. Briefly, cells were washed with PBS and suspended in lysis buffer provided by the supplier. Aliquots were taken from each cell lysate, and the amount of GAPDH proteins present in the lysates was determined and used for normalization. GTP-bound forms of Rac were then pulled down from lysates using reagents provided by the supplier, following the recommended instructions. Proteins present in total cell lysates or Rac pull-down samples were separated by SDS-PAGE (12%) and transferred onto a nylon membrane. Western blotting was performed using antibodies against Rac1, according to the ECL protocol provided by the suppliers. Luminescence of Rac1 bands was quantified using the GE ImageQuant LAS 4000 (GE Healthcare Life Science, Sweden).

Acknowledgements

We thank members of Gene Technology Center in Kumamoto University for their technical assistance.